HUNGARIAN GROUP OF *fib*

CONCRETE STRUCTURES

ANNUAL TECHNICAL JOURNAL

2025

Vol. 26

Scientific Committee

György L. Balázs (HU), Chairman, BME
Sándor Sólyom (HU), Co-Chairman, BME
Kálmán Koris (HU), Co-Chairman, BME

Advisory Board members of the Scientific Committee

Marco di Prisco (IT), Politecnico di Milano
Giovanni Plizzari (IT), Università di Brescia
Bruno Massicotte (CA), Polytechnique Montréal
Jean-Philippe Charron (CA), Polyt. Montréal
Fausto Minelli (IT), Università di Brescia
Barzin Mobasher (US), Arizona State Univ

Members

Alejandro Perez Caldentey (ES)
Ana Elisabete P.G.A. Jacintho (BR)
Antoine Naaman (US)
Atef Daoud (TN)
Avraham Dancygier (IL)
Billy Boshoff (ZA)
Brecht Vandevvere (BE)
Bryan Barragan (FR)
Christian U. Grosse (DE)
David Fernandez-Ordoñez (CH)
Dirk Schlicke (AT)
Ekkehard Fehling (DE)
Elena Vidal Sarmiento (BE)
Éva Lublóy (HU)
Filippo Medeghini (DE)
Frank Dehn (DE)
Gabriele David Bocchino (IT)
Gábor Csorba (HU)
Gonzalo Ruiz López (ES)
Gustavo Parra Montesinos (US)
Gyorgy Farkas (HU)
Ildiko Merta (AT)
Imre Kovács (HU)
Ingrid Lande (NO)
István Sajtos (HU)
István Völgyi (HU)
Jan Cervenka (CZ)
Jan Vorel (CZ)
Jean Michel Torrenti (FR)
Joaquim Barros (PT)
Juan Navarro Gregori (ES)
Hans Beushausen (ZA)
Károly Péter Juhász (HU)
Klaus Holschemacher (DE
Liberato Ferrara (IT)
Lin Wan-Wendner (BE)
Lucie Vandewalle (BE)
Luis Segura (UY)
Matteo Colombo (IT)
Marek Salamak (PL)
Naser Alimrani (CA)
Nemy Banthia (CA)
Nicola Buratti (IT)
Nicola Tosic (ES)
Nilufer Ozyurt (TR)
Norbert Randl (AT)
Oliver Fenyvesi (HU)
Paolo Martinelli (IT)
Pedro Serna Ros (ES)
Peter Mark (DE)
Péter Schaul (HU)
Pierre Rossi (FR)
Raul Luis Zerbino (AR)
Ralf Winterberg (DE)
Ravindra Gettu (IN)
Robert Németh (HU)
Roman Wan-Wendner (BE)
Rutger Vrijdaghs (BE)
Salem G. Nehme (HU)
Sébastien Wolf (LU)
Sherif Abdel Aziz Yehia (AE)
Silvia Ientile (FR)
Stefan Bernard (AU)
Tamás Kovács (HU)
Tamon Ueda (JP)
Terje Kanstad (NO)
Todd Clarke (AU)
Tor Arne Martius-Hammer (NO)
Viktor Gribniak (LT)
Viktor Hlavicka (HU)
Vincent Oettel (DE)
Yuri Karinski (IL)
Zoltán Orbán (HU)

MŰEGYETEM 1782

Organizer

Budapest University of Technology and Economics (BME),
Faculty of Civil Engineering

Supported by:

ACI - https://www.concrete.org

fib - www.fib-international.org

RILEM - https://www.rilem.net

Dates

December 15, 2025	Submission of abstracts
January 10, 2026	Extended Abtract deadline
January 15, 2026	Acceptance of abstracts
March 31, 2026	Full paper submission
May 31, 2026	Full paper review
July 1, 2026	Full paper acceptance

Registration fee

Early / regular	600 / 700 EUR
Student / PhD student	300 EUR
Banquet	100 EUR
Early bird ends	July 15, 2026

Registration fee includs: Welcome cocktail, Coffee breaks, Lunches and Pre-Proceedings. It is required for every presentation to have a separate registration.

Organizing Committee

Sándor Sólyom (HU), Chairman, BME
Kálmán Koris (HU), Co-Chairman, BME
György L. Balázs (HU), Co-Chairman, BME
János Czirják (HU)
Ahmed Seyam (UK) Adrienn Für-Kovács (HU) Jorge Luis Campoverde (HU)
András Bíró (HU) Tibor Mihucz (HU) Katalin Kopecskó (HU)
Bálint Somlai (HU) Csaba Miklós (HU) Marie Reymond (CH)
Corinne Bottollier Depois (CH), Ronny Ramiro Almeida Vasquez (HU)
Hatem Affez (HU) László Polgár (HU) László Sipos (HU) Szabolcs Szinvai (HU)

ACI-*fib*-RILEM FRC-UHPFRC Workshop

„Fibre Reinforced Concrete – From Design to Structural Applications"

Sept. 28 to 30, 2026 Budapest, Hungary

ACI-*fib*-RILEM FRC WORKSHOP BUDAPEST 2026

Steel fiber reinforced concrete thin shell structure
Oceanographic Park Restaurant. *City of Arts and Sciences*, Valencia (2002)
Based on blueprint of Felix Candela, by: A. Domingo, C. Lázaro, P. Serna

CONCRETE STRUCTURES
Journal of the Hungarian Group of ***fib***

Founded by: Hungarian Group of ***fib***
Publisher: Hungarian Group of ***fib***
(***fib*** = International Federation for Structural Concrete)

Editorial office:
Budapest University of Technology and Economics (BME)
Department of Construction Materials and Technoligies
Műegyetem rkp. 3., H-1111 Budapest
Phone: +36-1-463 4068
Fax: +36-1-463 3450
WEB http://www.fib.bme.hu
WEB editor: András Bíró

Layout and print: Csaba Halmai, Navigar Ltd.

Printed in 100 copies and web.

HU ISSN 2062-7904
online ISSN: 1586-0361

Cover photo:
Dancing House, Praha
Photo: György L. Balázs

CONTENT

Sponsors:

Railway Bridges Foundation, ÉMI Nonprofit Ltd., HÍDÉPÍTŐ Co., Holcim Hungary Co., MÁV Co., MSC Consulting Co., Lábatlani Vasbetonipari Co., Pont-*TERV* Co., UVATERV Co., MÉLYÉPTERV KOMPLEX Engineering Co., SW Umwelttechnik Hungary Ltd., Betonmix Consulting Ltd., BVM Épelem Ltd., CAEC Ltd., Pannon Freyssinet Ltd., STABIL PLAN Ltd., BME Dept. of Structural Engineering, BME Dept. of Construction Materials and Technologies

PERFORMANCE OF MECHANICALLY ACTIVATED VOLCANIC TUFF AS A TYPE II ADDITIVE: MECHANICAL EVOLUTION AND DURABILITY IN AGGRESSIVE ENVIRONMENTS

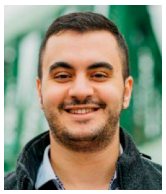


https://doi.org/10.32970/CS.2025.1.1

Affes Hatem – Salem G. Nehme

The degradation of sewage infrastructure by biogenic sulfuric acid poses a critical challenge for sustainable construction. This study evaluates a mechanically activated volcanic tuff (Cyment L100) as a Type II additive, specifically targeting durability in aggressive wastewater environments. Mechanical evolution and acid resistance (pH 1) were tested for mixtures containing 20% and 40% replacement in CEM I and CEM II systems. Results show that while early strength decreased, CEM I mixtures achieved significant recovery (75 MPa at 56 days). Crucially, acid testing revealed an inversion of the degradation mechanism: while standard Portland cement suffered severe erosion (-1.32% mass loss), the volcanic tuff mixture exhibited mass gain (+1.0%) and retained 100% of its flexural strength. Although frost resistance tests indicated a need for air-entrainment in freeze-thaw zones, the results position this volcanic binder as a specialized, high-durability solution for lining sewage pipelines and wastewater treatment plants (Exposure Class XA3), offering superior resistance to chemical attack compared to standard binders.

Keywords: Volcanic Tuff, Supplementary Cementitious Materials, Concrete Durability, Freeze–Thaw Resistance, Chloride Migration, Acid Resistance

1. INTRODUCTION

Concrete is the most widely used construction material globally, and its production is a major contributor to anthropogenic carbon dioxide emissions, primarily due to the calcination process in clinker manufacturing (Scrivener et al., 2018). To address this, the industry is increasingly adopting Supplementary Cementitious Materials (SCMs) such as fly ash, slag, and natural pozzolans. Volcanic tuffs, abundant in many regions including the Carpathian Basin, possess pozzolanic properties—specifically reactive amorphous silica and alumina—that allow them to react with calcium hydroxide (CH) to form secondary Calcium-Silicate-Hydrate (C-S-H) gels.

Beyond carbon reduction, a critical challenge in modern infrastructure is the rapid deterioration of sewage and wastewater systems due to Biogenic Sulfuric Acid (BSA) corrosion. In these environments, bacteria convert sulfates into sulfuric acid, leading to pH levels as low as 1–2, which rapidly dissolves calcium hydroxide in standard Portland cement. Therefore, developing binders that consume calcium hydroxide through pozzolanic activity is essential for extending the service life of wastewater networks.

This study evaluates "Cyment L100," a mechanically activated volcanic tuff-based Type II additive. While previous studies have established the general pozzolanic potential of volcanic rocks, this research focuses on the specific trade-offs between chemical durability (acid resistance), transport properties (watertightness), and physical durability (frost resistance) in high-performance concrete. We hypothesize that the pore refinement caused by the pozzolanic reaction enhances chemical resistance but may alter the air-void system, potentially compromising freeze-thaw stability in the absence of air-entraining agents.

The objective is to determine the optimal replacement level (20% vs. 40%) and binder compatibility (CEM I vs. CEM II) to maximize sustainability without sacrificing critical durability metrics required for aggressive exposure classes (XA3, XF4).

2. EXPERIMENTAL PROGRAM

2.1. Materials

Two types of cement supplied by Duna-Dráva Cement Kft. were used:

2.1.1. CEM I 52.5 N

A rapid-hardening Portland cement was selected to provide a binder matrix with high alkalinity and abundant calcium hydroxide (CH). This ensures an optimal environment for the pozzolanic reaction, allowing for the assessment of the intrinsic reactivity of the Cyment L100 additive without the interference of competitive secondary reactions.

2.1.2. CEM II/A-S 42.5 N: A Portland-slag cement containing 6–20% blast furnace slag

A Portland-slag cement was chosen to represent current low-carbon industry standards. This binder allows for the

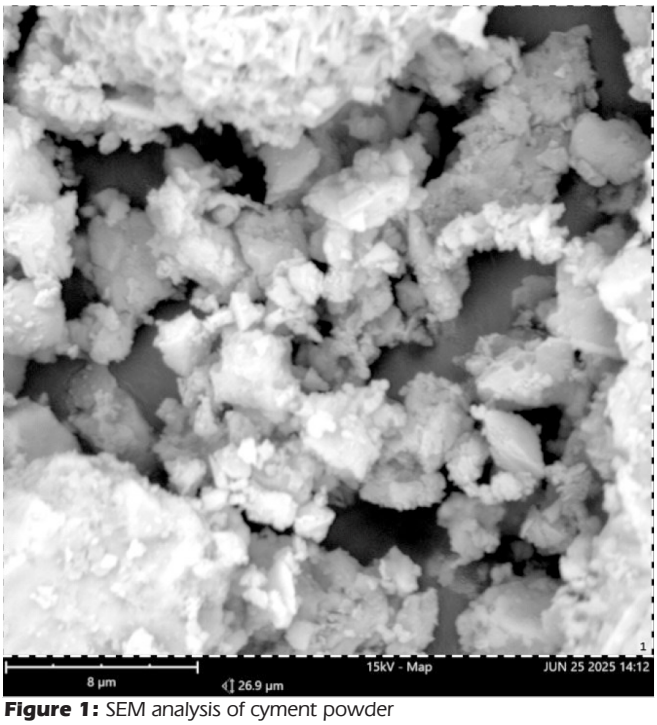

Figure 1: SEM analysis of cyment powder

investigation of 'multi-blend' compatibility; specifically, whether the volcanic tuff can be effectively used in systems where the clinker factor is already reduced by blast furnace slag (Siddique, R. 2012). This combination evaluates the risks of 'clinker dilution' and the competitive demand for calcium hydroxide between the slag and the volcanic tuff.

2.1.3. Cyment L100

Cyment L100 is a multi-component ground volcanic tuff-based additive, produced as a fine powder from pre-dried and mechanically conditioned volcanic tuff, metallurgical slag, and incineration ash. It is primarily used in concrete production, particularly for cast-in-situ and prefabricated structural concrete, where it enhances key properties such as non-permeability, heat reduction, and resistance to environmental aggressiveness.

Designed for use in combination with cements complying with EN 197-1, cyment L is assessed to provide a working life of at least 50 years when used in concrete. The manufacturer specifies its intended use as a type II addition in concrete. The manufacturing process follows conventional grinding techniques without additional treatments that would alter its performance, with further details provided in the manufacturer's documentation (Annex 1).

Scanning Electron Microscopy (SEM) analysis was conducted to verify the morphological characteristics of the mechanically activated volcanic tuff (Cyment). Contrary to the initial hypothesis of a spherical morphology typical of fly ash or silica fume, the micrographs reveal that the Cyment particles are predominantly **angular, irregular, and blocky** with sharp fracture edges *(Fig. 1)*.

This morphology is consistent with the comminution process of natural rock, confirming its origin as a ground volcanic tuff. The images display a polydisperse particle size distribution, where finer dust-like particles ($< 2 \mu m$) adhere to the surfaces of larger angular fragments ($10–50 \mu m$). While the lack of spherical shape may increase water demand due to higher inter-particle friction, the rough surface texture and wide gradation likely contribute to a dense particle packing effect, enhancing the physical impermeability of the binder matrix.

Powder X-ray diffraction (XRD) is a powerful analytical technique used primarily for identifying the crystallographic structure, phase composition, and physical properties of a material. It is particularly useful in materials science, chemistry, geology, and engineering for several key applications. The XRD analysis of the cyment L100 indicates the presence of reactive amorphous phases alongside crystalline quartz (SiO_2) and hematite (FeO).

- Iron Oxide (Wüstite, FeO): This phase contributes to the materials overall structure and potentially to its reactivity in cement systems.

Figure 2: X-ray diffraction of cyment powder

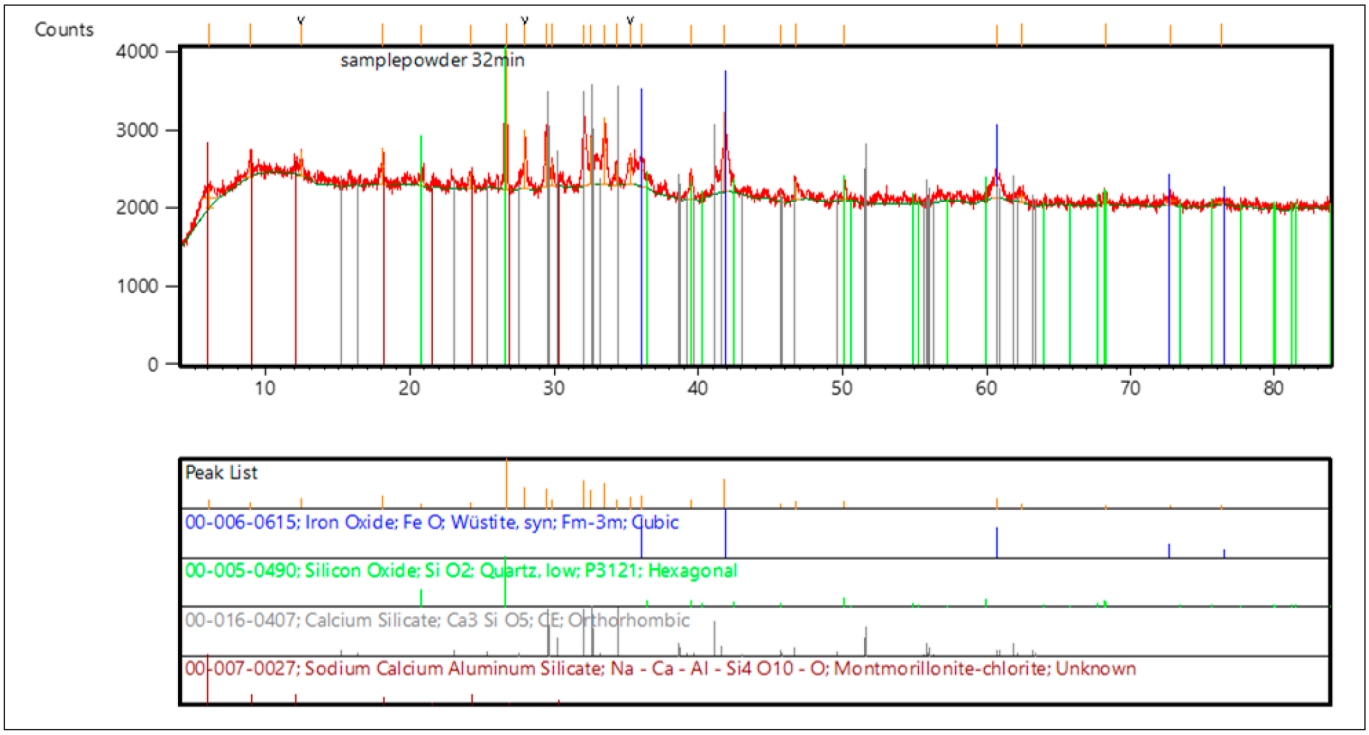

- Silicon Oxide (Quartz, SiO_2): A critical component that likely contributes to the pozzolanic reactivity of cyment, particularly in later-stage strength development.
- Calcium Silicate (Ca_3SiO_5): This phase resembles alite, the primary strength-developing component in Portland cement, suggesting cyment contains cementitious properties inherently.
- Sodium Calcium Aluminum Silicate (Montmorillonite-chlorite): A complex aluminosilicate phase that may contribute to the materials reactivity with calcium hydroxide during cement hydration.

These phases suggest the presence of oxides and silicates, commonly found in geological or construction materials like cement or clays. Each phase is indexed with a reference number for verification against known standards. The XRD profile *(figure 2)* provides insights into the sample's mineral composition, as the peak positions and intensities correlate with specific crystal structures. The material analyzed in the document appears to be crystalline rather than amorphous. This conclusion is based on the presence of distinct peaks in the XRD pattern. Crystalline materials produce sharp, well-defined peaks in an XRD analysis due to the orderly arrangement of atoms in their structure. Amorphous materials, on the other hand, lack this long-range order and typically show broad, diffuse humps rather than distinct peaks. The sharp peaks identified, corresponding to specific minerals like quartz and Wüstite, confirm its crystalline nature.

2.2. Concrete mix design

Six concrete mix designs were developed for this study, divided into two series based on cement type. For each cement type, three mixes were prepared: a standard reference mixture without Cyment (designated as A-0 or B-0), a mixture with 20% cement replacement by Cyment (A-20% or B-20%), and a mixture with 40% cement replacement (A-40% or B-40%). The CEM I 52.5 N series was formulated with a cement content of 380 kg/m^3 in the reference mixture, while the CEM II A-S 42.5 N series contained 340 kg/m^3 of cement in its reference mixture.

In the Cyment-containing mixtures, 20% or 40% of the cement weight was replaced with Cyment L100, with all other components remaining consistent within each series. This replacement strategy allowed for direct comparison of the effects of Cyment addition on concrete properties without the influence of other variables.

The concrete mixtures were prepared using a consistent aggregate framework across all mix designs. Sika ViscoCrete 4025 was employed as a plasticizer to achieve the target consistency class (F4) for all mixtures. The water-to-cement ratios were maintained at 0.4 for CEM I mixtures and 0.5 for CEM II mixtures, ensuring comparability within each cement type series while acknowledging the inherent differences between the two cement types.

3. METHODOLOGY

A comprehensive testing program was implemented to evaluate various properties of fresh and hardened concrete. Fresh concrete tests included consistency evaluation through spread tests according to MSZ EN 12350-5:2019 and bulk density measurements following MSZ EN 12350-6:2019. The consistency was adjusted using a plasticizer to achieve the F4 consistency class for all mixtures, ensuring workability comparability across the different compositions. Hardened concrete properties were evaluated through several standardized tests.

Compressive strength was determined on 150 mm cube specimens at ages of 2, 28, and 56 days according to MSZ EN 12390-3:2019, with three specimens tested per mixture and age. Watertightness testing was conducted following MSZ EN 12390-8:2019, providing insights into the permeability characteristics of the different mixtures.

Durability aspects were assessed through frost resistance testing (flange peeling in 3% NaCl medium) according to MSZ CEN/TS 12390-9:2018, chloride ion penetration testing using a migration apparatus and silver nitrate spray indicator, and acid resistance evaluation involving 8-week exposure to pH 1 sulfuric acid.

For the acid resistance test, specimens were prepared as 70 × 70 × 250 mm prisms, with three specimens per mixture subjected to standard conditions (submerged in water) and three to acidic conditions, followed by assessment of mass change and strength properties after the exposure period.

4. RESULTS

4.1. Fresh properties

All mixtures were adjusted to meet the target F4 consistency class (flow diameter 490–550 mm) by varying the superplasticizer dosage. As shown in Table 2 and Table 3, the addition of volcanic tuff (Cyment) had a negligible impact on fresh concrete density, with values remaining within the range of 2,350–2,390 kg/m^3.

Notably, in the CEM I series, the 40% replacement mixture (A-40) required slightly less superplasticizer (2.74 kg/ m^3) than the reference (3.04 kg/m^3) to achieve similar workability (590 mm vs. 570 mm).

4.2. Compressive strength

Compressive strength tests were conducted on 150 mm cubic specimens in accordance with MSZ EN 12390-3:2019. Three

Table 1: Mix Proportions ()

Mix ID	Binder	Cement (kg/m^3)	Cyment (kg/m^3)	Water (kg/m^3)	Replacement
A-0 (Ref)	CEM I 52.5 N	380	0	152	0%
A-20		304	76	152	20%
A-40		228	152	152	40%
B-0 (Ref)	CEM II/A-S	340	0	170	0%
B-20		272	68	170	20%
B-40		204	136	170	40%

Table 2: Fresh concrete properties of CEM I 52.5 N mixtures

Mix ID	Cement Replacement	Superplasticizer	Slump Flow	Fresh Density	Temperature
	(%)	(kg/m³)	(mm)	(kg/m³)	(∘C)
A-0 (Ref)	0%	3.04	570	2,390	21
A-20	20%	3.04	600	2,390	21.2
A-40	40%	2.74	590	2,370	21.4

Table 3: Fresh concrete properties of CEM II/A-S 42.5 N mixtures

Mix ID	Cement Replacement	Superplasticizer	Slump Flow	Fresh Density	Temperature
	(%)	(kg/m³)	(mm)	(kg/m³)	(°C)
B-0 (Ref)	0%	1.7	520	2,380	22.1
B-20	20%	2.31	550	2,370	22.3
B-40	40%	2.04	540	2,350	22.4

specimens were tested for each mixture at every testing age (2, 28, and 56 days).

In the case of mixtures made with CEM I 52.5 N cement, the addition of Cyment resulted in a distinct retardation of early-age strength. At 2 days, the mixtures exhibited a 40–50% strength deficit compared to the reference. However, the pozzolanic reaction accelerated significantly thereafter; by 28 days, the strength gap narrowed to 12–22%. At 56 days, the mixtures maintained structural-grade strengths, with the gap stabilizing between 10–20% for both replacement levels *(Figure 3)*.

For the CEM II series, the interaction between the additive and the slag-blended cement varied significantly by dosage. The 20% replacement mixture (B-20) showed excellent compatibility, initially lagging by 15% at 2 days but fully recovering to match (and momentarily exceed) the reference strength by 28 days (101.6%). Conversely, the 40% replacement (B-40) exhibited a sharp drop in early strength (50% deficit at 2 days) and stabilized at approximately 20% lower strength than the reference at later ages *(Figure 3)*.

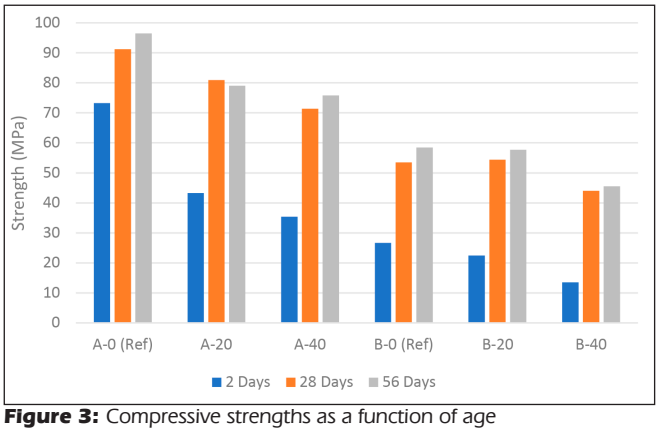

Figure 3: Compressive strengths as a function of age

4.2.1. Results for CEM I 52.5 N Series

Table 4.

4.2.2. Results for CEM II/A-S 42.5 N Series

Table 5.

4.3. Watertightness

The watertightness test of the solidified concrete test specimen was carried out on the basis of the MSZ EN 12390-8:2019 standard.

In the CEM I series, Cyment addition clearly improved watertightness. The average penetration depth decreased from 23.6 mm (Reference) to 19.5 mm (A-20) and 18.3 mm (A-40). This corresponds to a 17–22% improvement in impermeability. However, in the CEM II series, the opposite effect was observed, with penetration depths increasing significantly in the blended cement mixtures.

Table 4: Compressive strength development of mixtures with CEM I 52.5 N

Mix ID	2 Days		28 Days		56 Days	
	Strength (MPa)	Rel. (%)	Strength (MPa)	Rel. (%)	Strength (MPa)	Rel. (%)
A-0 (Ref)	73.29	100	91.19	100	96.5	100
A-20	43.29	59.1	80.89	88.7	79.07	81.9
A-40	35.36	48.2	71.38	78.3	75.85	78.6

Table 5: Compressive strength development of mixtures with CEM II/A-S 42.5 N

Mix ID	2 Days		28 Days		56 Days	
	Strength (MPa)	Rel. (%)	Strength (MPa)	Rel. (%)	Strength (MPa)	Rel. (%)
B-0 (Ref)	26.64	100	53.52	100	58.46	100
B-20	22.45	84.3	54.39	101.6	57.74	98.8
B-40	13.5	50.7	43.99	82.2	45.56	77.9

Table 6: Watertightness results of mixtures

Mix ID	Average Depth (mm)	Relative to Ref. (%)
A-0 (Ref)	23.6	100%
A-20	19.5	83%
A-40	18.3	78%
B-0 (Ref)	15.3	100%
B-20	20.4	133%
B-40	27.4	179%

Table 7: Cumulative scaling mass loss after 56 freeze-thaw cycles

Mix ID	Scaling (g/m^2)	Relative to Ref. (%)	Visual Assessment
A-0 (Ref)	1,399	100%	Slight Scaling (Acceptable)
A-20	4,581	327%	High Scaling (Pass*)
A-40	4,957	354%	High Scaling (Pass*)
B-0 (Ref)	1,825	100%	Slight Scaling (Acceptable)
B-20	7,896	432%	Severe Scaling
B-40	>10,000	--	FAILED (Disintegration)

4.4. Frost resistance (Flange peeling)

The freeze-thaw resistance was evaluated using the slab test method (CEN/TS 12390-9:2018). Specimens were exposed to 56 freeze-thaw cycles in the presence of a 3% NaCl de-icing solution.

4.5. Chloride migration

The resistance to chloride ingress was evaluated using the non-steady-state migration test (similar to NT BUILD 492). The penetration depth (X_d) was measured at 28 days and 56 days to capture the evolution of the pore structure.

4.6. Acid resistance

The acid resistance testing, involving 8-week exposure to pH 1 sulfuric acid, revealed notable differences in performance between mixtures with and without Cyment. In the CEM I series, the standard mixture experienced a mass loss of approximately 1.5%, corresponding to visible surface deterioration. In contrast, specimens with Cyment addition showed no mass loss during the acid exposure, indicating superior acid resistance.

Six specimens (70 × 70 × 250 mm) were prepared from each mixture. Three reference specimens were stored under water. The acidic medium was adjusted to pH 1. The medium was changed weekly after measuring the specimens masses.

The reference mixture (A-0) *(Figure 4)* was the only formulation to suffer mass loss (-1.32%). In sharp contrast,

Figure 4: CEM I specimens after the acid test

Figure 5: CEM II specimens after the acid test

Table 8: chloride migration depths

Mix ID	28-Day Depth (mm)	56-Day Depth (mm)	Evolution (28d → 56d)	Performance at 56d
A-0 (Ref)	11.9	12.9	+8.4% (Stable)	Reference Baseline
A-20	11.6	11.8	+1.7% (Stable)	Equivalent to Ref
A-40	13.8	9.4	-31.9% (Improvement)	Best Performance
B-0 (Ref)	17.1	18.8	+9.9% (Degradation)	High Permeability
B-20	14.2	14.9	+4.9% (Stable)	Better than Ref
B-40	22.6	15.9	-29.6% (Improvement)	Improved vs 28d

Table 9: Average Mass Change after 8 Weeks (Acid vs. Water)

Mix ID	Water Storage (Control)	Acid Storage (1% H_2SO_4)	Durability Status
A-0 (Ref)	+1.0 g (+0.03%)	-38.7 g (-1.32%)	Surface Erosion (Mass Loss)
A-20	+22.1 g (+0.75%)	+15.2 g (+0.51%)	Intact (Mass Gain)
A-40	+20.4 g (+0.69%)	+31.9 g (+1.09%)	Intact (Mass Gain)
B-0 (Ref)	+10.3 g (+0.36%)	+15.6 g (+0.53%)	Intact (Mass Gain)
B-20	+25.9 g (+0.89%)	+34.4 g (+1.16%)	Intact (Mass Gain)
B-40	+20.6 g (+0.71%)	+36.2 g (+1.25%)	Intact (Mass Gain)

Table 10: *Residual Compressive Strength after 8 Weeks in 1%*

Mix ID	Standard Strength (MPa)	Post-Acid Strength (MPa)	Retention Index (%)	Performance vs Ref
A-0 (Ref)	89.9	54.6	60.70%	Severe Degradation
A-20	77.2	58.8	76.20%	Moderate Protection
A-40	71.2	64.9	91.20%	High Protection
B-0 (Ref)	60.3	54.8	90.90%	Inherently Resistant
B-20	55.2	48.8	88.40%	Stable
B-40	46.4	43.9	94.60%	Stable (Low Strength)

Table 11: *Residual Flexural Strength after 8 Weeks in 1%*

Mix ID	Standard Strength (MPa)	Post-Acid Strength (MPa)	Retention Index (%)
A-0 (Ref)	4.76	4.49	94.30%
A-20	4.07	3.69	90.70%
A-40	4.37	4.49	102.7% (No Loss)
B-0 (Ref)	3.51	3.14	89.50%
B-20	3.5	3.43	98.00%
B-40	2.77	2.79	100.70%

the addition of Cyment (A-20 and A-40) completely arrested this erosion. Instead of losing mass, these mixtures gained mass (+0.5% to +1.0%).

The CEM II series (B-0, B-20, B-40) *(Figure 5)* consistently showed mass gain, confirming the inherent acid resistance of slag-based cements. The addition of Cyment further increased this mass gain. While this suggests no immediate erosion, the higher mass accumulation in B-40 (+1.25%) compared to B-0 (+0.53%) could indicate a higher volume of expansive product formation, which might lead to cracking over longer exposure periods (beyond 8 weeks).

4.7. Residual Mechanical Properties after Acid Exposure

The pure Portland cement (A-0) suffered a catastrophic loss of compressive strength, retaining only 60.7% of its capacity. As the replacement level increased, the degradation vanished. The A-40 mixture retained 91.2% of its strength. More importantly, in absolute terms, the A-40 mixture was stronger after acid attack (64.9 MPa) than the reference A-0 (54.6 MPa). Remarkably, the A-40 mixture showed no loss in flexural strength (102.7% retention).

The CEM II series exhibited high retention rates (88–95%) across all mixes, confirming that slag cements are inherently acid-resistant due to their lower calcium hydroxide content. However, the absolute strength of these mixtures remained significantly lower than the Cyment-modified CEM I mixtures (e.g., B-40 Acid Strength: 43.9 MPa vs. A-40 Acid Strength: 64.9 MPa).

5. DISCUSSIONS

The experimental results define Cyment L100 as a chemo-dependent pozzolan whose performance is strictly governed by the alkalinity of the host binder and the specific exposure environment. This section analyzes the mechanisms driving the trade-offs between mechanical recovery (Uzalis, N., et al. 2005), transport properties, and chemical durability.

5.1. Fresh State and Early-Age Behavior

Unlike many natural pozzolans that increase water demand due to high specific surface area, Cyment L100 exhibited a neutral-to-positive effect on workability. In the CEM I series, the 40% replacement mixture (A-40) achieved the target F4 consistency (590 mm flow) with slightly lower superplasticizer dosage than the reference. This suggests that the mechanical activation process may optimize particle morphology, allowing the tuff to act as a lubricant or "ball bearing" in the fresh paste contrary to the typical water-demand increase observed with some natural pozzolans.

However, the "Dilution Effect" was evident at early ages. By replacing rapid-hardening clinker with slower-reacting volcanic tuff, the initial volume of hydration products was reduced, leading to a 40–50% strength deficit at 2 days across all mixtures. At this stage, the volcanic tuff acts primarily as an inert filler, as the alkalinity of the pore solution is not yet sufficient to trigger the dissolution of amorphous silica.

5.2. Mechanical Evolution and Activator Starvation

The subsequent strength development highlights the "Critical Clinker Factor".

The experimental data defines Cyment L100 as a chemo-dependent pozzolan whose mechanical efficiency is strictly governed by the alkalinity of the host binder.

- In High-Alkalinity Environments (CEM I): Cyment transitions from a filler to a binder. The abundance of calcium hydroxide (CH) provided by the pure Portland clinker drives the pozzolanic reaction, allowing the A-40 mixture to recover from 35 MPa (2 days) to 75 MPa (56 days).
- In Competitive Environments (CEM II): The B-40 mixture (CEM II + 40% Cyment) revealed a phenomenon of "Activator Starvation." The simultaneous demand for alkalis by both the slag (inherent in CEM II) and the high volume of Cyment exceeded the system's capacity. This "Double Negative" effect arrested hydration, leaving the Cyment largely unreacted and resulting in a permanent strength deficit (Turk, k., et al. 2007).

5.3. Transport Properties: The "Late-Blocking" Effect

The impact of Cyment on fluid transport revealed a strong time-dependency, confirming its slow reaction kinetics.

In the Chloride Migration test, the A-40 mixture initially performed worse than the reference at 28 days (13.8 mm vs. 11.9 mm), behaving as a porous matrix. However, a dramatic transformation occurred between 28 and 56 days, where the penetration depth dropped by 32% to just 9.4 mm. This "Late-Blocking" effect confirms that once the volcanic tuff dissolves and reacts with calcium hydroxide, the secondary C-S-H products effectively precipitate within the capillary network (Massazza, F. 2022). This mechanism correlates directly with the watertightness results, where the A-40 mixture achieved the densest microstructure among all mixes, but only after sufficient curing time.

Conversely, in the CEM II series, this blocking mechanism failed. The B-40 mixture exhibited increased permeability, further evidence that without sufficient CH to activate the tuff, the particles serve only to disrupt the binder matrix rather than refine it (Khan, M. I. 2012).

5.4. The Durability Paradox: Frost vs. Chemical Resistance

The most significant finding of this study is the sharp divergence between physical and chemical durability performance.

5.4.1. Freeze-Thaw Vulnerability (Physical Failure)

While Cyment improved impermeability in CEM I, it drastically reduced frost resistance. The failure mechanism appears to be twofold:

1. Air-Void Destabilization: Frost resistance relies on a network of microscopic air bubbles to relieve hydraulic pressure (Valcuende, M., & Parra, C. 2010). The high volume of fine volcanic tuff particles (76–152 kg/m^3) likely filled these voids or destabilized the entrained air during mixing.
2. Pore Connectivity: Although Cyment refined the chemical porosity (blocking chloride ions), it appears to have created a capillary network that, while finer, remains saturable. When this refined system freezes, the hydraulic pressure cannot escape, leading to surface scaling.

The catastrophic failure of the B-40 mixture serves as a warning against using high-volume pozzolans in low-clinker systems without air entrainment; the weak binder matrix simply disintegrated under expansive ice forces.

The experimental data reveals a critical vulnerability in the use of volcanic tuff without air-entrainment adjustments. cyment L100 significantly increases the scaling potential of concrete. While it acts as a pore-blocker for fluids (improving watertightness), it does not provide freeze-thaw protection. Consequently, for applications exposed to de-icing salts (Exposure Class XF4), Cyment mixtures must be air-entrained or limited to lower replacement levels (<20%) to prevent surface degradation.

5.4.2. Acid Resistance (Chemical Shield)

In contrast to the physical failure under frost, Cyment provided a decisive advantage against chemical attack. In the sulfuric acid exposure test, the pure CEM I reference suffered severe degradation, losing mass and 40% of its compressive strength due to the rapid dissolution of calcium hydroxide.

Cyment effectively reversed this degradation. The A-40 mixture not only prevented mass loss but retained 91% of its compressive strength and 100% of its flexural strength. By consuming the soluble calcium hydroxide; the primary target for acid attack in **sewage environments**; cyment effectively mitigates the risk of **biogenic corrosion**. The formation of a dense, chemically stable matrix suggests that Cyment-modified concrete is particularly suitable for **Exposure Class XA3** (highly aggressive chemical environments), common in industrial and municipal wastewater facilities.

6. FINDINGS

The most distinct advantage of the Cyment-modified binder is its exceptional resistance to sulfuric acid (pH 1), identifying it as a premium material for **sewage infrastructure**. While standard CEM I concrete suffered severe surface erosion (-1.32% mass loss), the volcanic tuff mixture inverted this mechanism, leading to mass gain (+1.0%) and the retention of **100% of flexural strength**. This confirms that Cyment acts as an effective chemical shield against biogenic acid corrosion in wastewater treatment tanks and pipes.

The study establishes a definitive boundary for usage. Cyment acts as a "chemo-dependent" additive that requires a high-alkalinity host. In **CEM I systems**, it contributes to strength recovery (75 MPa at 56 days); however, in low-clinker **CEM II systems**, it induces "activator starvation," leading to arrested hydration.

A critical divergence was identified between chemical and physical durability. The same pore refinement that blocked chloride ingress (-32% depth) created a capillary structure vulnerable to freezing pressure. Therefore, this study mandates that for **Exposure Class XF4**, Cyment usage must be coupled with air-entrainment or limited to <20% replacement to prevent scaling failure.

At 40% replacement in CEM I, the material offers a viable strategy for reducing embodied carbon by **roughly 33%** without compromising long-term mechanical performance, provided the curing duration is sufficient to overcome the early-age dilution effect.

7. REFERENCES

Cyment: Fewer emissions, more sustainability: (n.d.). Retrieved from https://www.cyment.eu/en/

MSZ EN 197-1:2011. Cement – Part 1: Composition, specifications and conformity criteria for common cements. European Committee for Standardization.

MSZ EN 12390-3:2019. Testing hardened concrete – Part 3: Compressive strength of test specimens. European Committee for Standardization.

MSZ EN 12390-8:2019. Testing hardened concrete – Part 8: Depth of penetration of water under pressure. European Committee for Standardization.

CEN/TS 12390-9:2016. Testing hardened concrete – Part 9: Freeze-thaw resistance - Scaling. European Committee for Standardization.

Scrivener, K. L., John, V. M., & Gartner, E. M. (2018). Eco-efficient cements: Potential economically viable solutions for a low-CO2 cement-based materials industry. Cement and Concrete Research, 114, 2–26.

Siddique, R. (2012). Effect of volcanic ash on the properties

of cement paste and mortar. Resources, Conservation and Recycling, 56, 66–70.
Massazza, F. (2002). Pozzolana and pozzolanic cements. In Lea's Chemistry of Cement and Concrete (4th ed., pp. 471–631). Butterworth-Heinemann.
Uzalis, N., et al. (2005). The effect of volcanic tuff on the strength and durability of concrete. Cement and Concrete Research, 35(9), 1785-1793.
Khan, M. I. (2012). Permeability and chloride penetration resistance of concrete containing natural pozzolan. Journal of Materials in Civil Engineering, 24(11).
Valcuende, M., & Parra, C. (2010). Natural products as a substitute for microsilica in high-performance concrete: Frost resistance. Construction and Building Materials, 24(12).
Allahverdi, A., & Škvára, F. (2000). Acidic corrosion of hydrated cement-based materials. Ceramics – Silikáty, 44(3), 114–120.
Turk, K., et al. (2007). Sulfate resistance of blended cements containing natural pozzolan and fly ash. Construction.
Massazza, F. (2002). Pozzolana and pozzolanic cements. In Lea's Chemistry of Cement and Concrete (4th ed., pp. 471–631). Butterworth-Heinemann.

Affes Hatem, MSc Structural engineer
Budapest University of Technology and Economics, Budapest, Hungary. From Sfax, Tunisia, currently pursuing his PhD at the Budapest University of Technology and Economics, Hungary. Having completed his Bachelor's and Master's degrees in Hungary over the past decade, his work focuses on sustainable construction. Contact: affeshatem@edu.bme.hu

Salem Georges Nehme, PhD.
Budapest University of Technology and Economics, Budapest, Hungary. Serves at the Budapest University of Technology and Economics, Hungary. Acting as a PhD supervisor, his research expertise centers on advanced construction materials and concrete durability. Contact: salem.nehme@emk.bme.hu

COMPARATIVE ANALYSIS OF FIRE CURVES AND STRUCTURAL PERFORMANCE: ISO 834, HYDROCARBON, AND ELECTRIC VEHICLE (EV) FIRES


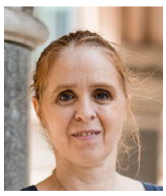

Bara Alseid - Éva Lublóy

https://doi.org/10.32970/CS.2025.1.2

The increasing complexity of fire hazards in modern infrastructure, particularly in industrial environments and parking garages, demands a comprehensive understanding of fire behavior and its impact on structural materials. This study provides a detailed comparison of three critical fire curves: ISO 834, Hydrocarbon (HC), and Electric Vehicle (EV) fires, focusing on their effects on concrete, steel, and composite materials. While ISO 834 remains the standard for typical building fires, the rapid temperature rise of hydrocarbon fires, reaching 1100 °C in under five minutes, and the prolonged heat exposure of EV fires, exceeding 1200 °C, pose significant challenges for modern construction. Notably, the similarity between HC and EV fire behaviors allows for the adaptation of HC fire parameters for evaluating EV fires, offering a practical and efficient approach for assessing their effects on concrete structures. The findings reveal that hydrocarbon fires result in rapid spalling of concrete and buckling of steel, particularly in confined environments such as tunnels and industrial facilities, where heat buildup exacerbates structural vulnerabilities. EV fires, driven by the thermal runaway of lithium-ion batteries, cause prolonged material degradation, increasing the risk of structural collapse in parking garages and similar settings. To address these challenges, this study recommends the implementation of fireproof coatings, heat-resistant additives for concrete, and advanced ventilation and fire suppression systems. Furthermore, building codes and fire safety standards must be updated to reflect the unique risks posed by these fire scenarios, ensuring that modern structures are adequately equipped to withstand their demands. By adapting HC fire parameters for EV fire evaluations, engineers can streamline safety assessments while maintaining robust structural integrity, paving the way for safer and more resilient infrastructure capable of withstanding the evolving fire hazards of the modern world.

Keywords: Hydrocarbon fie, ISO 834 fire, electric vehicle fire

1. INTRODUCTION

Fire safety is a fundamental aspect of structural engineering, where the ability of materials and structures to withstand fire exposure can prevent catastrophic failures. Traditionally, fire resistance has been assessed using the ISO 834 standard fire curve, which simulates a relatively predictable building fire. The ISO 834 curve models a fire that gradually increases in temperature, reaching around 840 °C in the first 30 minutes and eventually rising to 1200 °C over several hours (ISO 834-1, n.d.). This curve is central to many building codes and forms the basis for evaluating how materials like concrete, steel, and composites behave when exposed to high temperatures. However, as industrial activities and emerging technologies such as electric vehicles (EVs) become more prevalent, new fire hazards have emerged that challenge the relevance of the ISO 834 curve.

The rise of hydrocarbon fires, commonly associated with environments such as chemical plants, tunnels, and refineries, represents a more aggressive fire scenario. The Hydrocarbon Modified (HC) fire curve is designed to model these extreme conditions, where temperatures can reach 1100 °C within just fifteen minutes (Caner et al., 2005). In addition to rapid temperature escalation, hydrocarbon fires place immense stress on building materials, causing spalling in concrete and rapid yield strength degradation in steel reinforcement. These fires pose an immediate risk to structural integrity, as materials degrade quickly and cannot withstand such intense heat for extended periods. In addition to hydrocarbon fires, the increased adoption of electric vehicles (EVs) has introduced a unique fire risk that differs significantly from traditional building or hydrocarbon fires. EV fires, particularly those involving lithium-ion batteries, present new challenges in fire safety. These batteries are prone to a phenomenon called thermal runaway, where an internal reaction causes the battery to rapidly heat and combust. The EV fire is characterized by a rapid rise in temperature, similar to hydrocarbon fires, but with added complexity due to prolonged burn times and the potential for re-ignition (Sun et al., 2020a). Once ignited, these fires can reach temperatures between 1000 °C and

1200 °C within a few minutes, generating significant amounts of heat and toxic gases.

This presents serious risks in enclosed spaces such as underground parking garages or tunnels, where the heat and gases can cause severe structural damage. The EV fire thus, represents an evolving fire hazard that demands reconsideration of existing fire safety designs. The thermal runaway behavior and the challenges of extinguishing such fires make EV fires a particularly critical area for modern fire safety research. In comparison to the gradual temperature rise modeled by the ISO 834 fire curve, EV fires escalate rapidly, maintain high temperatures for longer, and present an ongoing risk even after initial extinguishment (Chen et al., 2021).

This shift in fire behavior, driven by hydrocarbon and EV fire scenarios, underscores the importance of updating fire resistance standards to reflect the more severe conditions posed by these modern fire types. The significance of comparing ISO 834, hydrocarbon, and EV fire lies in the vastly different temperature-time profiles and structural impacts each presents. The ISO 834 standard curve provides a gradual temperature increase, which allows for predictable modeling of how materials like concrete and steel degrade over time. However, this curve may not accurately reflect the more aggressive fire conditions found in industrial environments or the growing use of electric vehicles. These new fire types are marked by rapid temperature escalation and sustained high temperatures that can degrade materials much more quickly than anticipated under the ISO 834 curve when compared to the hydrocarbon fire scenario (Nguyen et al., 2025).

Understanding how each fire curve impacts material degradation is crucial for improving structural fire resistance in a wide range of environments. For instance, in tunnel fires fueled by hydrocarbons, the rapid heat escalation can cause concrete to experience spalling within minutes, significantly reducing its structural integrity. Similarly, the yield strength of steel decreases rapidly at temperatures above 500 °C, which can lead to catastrophic failures in steel-reinforced structures (Khoury, 2000; Zhao et al., 2025) but ultra-high-performance concrete behaves differently. A key property unique to concrete amongst structural materials is transient creep. Any structural analysis of heated concrete that ignores transient creep will yield erroneous results, particularly for columns exposed to fire. Failure of structural concrete in fire varies according to the nature of the fire; the loading system and the type of structure. Failure could occur from loss of bending or tensile strength; loss of bond strength; loss of shear or torsional strength; loss of compressive strength; and spalling of the concrete. The structural element should, therefore, be designed to fulfil its separating and/or load-bearing function without failure for the required period of time in a given fire scenario. Design for fire resistance aims to ensure overall dimensions of the section of an element sufficient to keep the heat transfer through this element within acceptable limits, and an average concrete cover to the reinforcement sufficient to keep the temperature of the reinforcement below critical values long enough for the required fire resistance period to be attained. The prediction of spalling – hitherto an imprecise empirical exercise – is now becoming possible with the development of thermohydromechanical nonlinear finite element models capable of predicting pore pressures. The risk of explosive spalling in fire increases with decrease in concrete permeability and could be eliminated by the appropriate inclusion of polypropylene fibres in the mix and/or by protecting the exposed concrete surface with a thermal barrier. There are three methods of assessment of fire resistance: (aIn the case of EV fires, prolonged exposure to extreme temperatures due to thermal runaway can weaken materials over an extended period, causing buckling, cracking, or even complete collapse (Chen et al., 2024) fire accidents due to impacts from the power battery located at the bottom of the electric vehicles are receiving increasing attention. Lithium-ion batteries, as the mainstream choice of power battery for electric vehicles solving the problem that they are prone to thermal runaway due to damage when impacted, are the key to preventing and controlling fire accidents in electric vehicles. To address the protective problem of the bottom power battery of electric vehicles when it is impacted by road debris, two new types of sandwich structures with an enhanced regular hexagonal structure and semicircular arch structure as the core layer, respectively, are innovatively proposed in this article. They are used to protect the bottom power battery of electric vehicles and are compared with the traditional homogeneous protective structure in terms of protective performance. A local finite element simulation (FEM. Comparing these fire curves also highlights the inadequacy of current fire safety standards in addressing the challenges posed by hydrocarbon and EV fires. Both fire types require new strategies for fire suppression, fireproofing, and material selection to mitigate the risks of rapid degradation and structural collapse.

This review aims to address gaps in current fire safety standards by conducting a detailed comparison of the ISO 834, Hydrocarbon, and Electric Vehicle (EV) fires, focusing on their temperature-time profiles, reduction factors, and structural impacts. The study integrates data from experimental results, case studies, and computational models to analyze how these fire scenarios affect essential construction materials such as concrete, steel, and composites.

The primary objectives of this review are to analyse the differences in temperature-time profiles between hydrocarbon and electric vehicle (EV) fires compared to the ISO 834 standard, focusing on peak temperatures, time to peak, and the severity of thermal loads imposed on structures. It also aims to investigate the degradation of materials such as concrete, steel, and composites under varying fire conditions, evaluating the reduction in their strength, stiffness, and mechanical properties at elevated temperatures. Furthermore, the study examines the structural impacts of these fire curves in real-world settings, including tunnels, parking garages, and industrial buildings, highlighting specific failures like spalling, buckling, and cracking due to high-temperature exposure. By addressing these critical aspects, the review will offer recommendations to enhance fire protection design and update fire resistance standards to better account for contemporary fire risks, especially those posed by hydrocarbon and EV fires.

2. FIRE CURVES OVERVIEW

Fire curves are crucial for understanding how different fire scenarios affect structural materials. These curves simulate the temperature-time profiles of fires and are used to predict the degradation of materials when exposed to high temperatures. *Table 1* summarize the comparison between different fires, where F*igure 1* shows a visual representation

Table 1: Peak Temperatures, Time to Peak, and Fire Duration

No.	Fire Curve	Peak Temperature (°C)	Time to Peak (minutes)	Fire Duration (hours)	References
1	ISO 834 Standard Fire	Gradual rise to **1000 °C** over 60-90 minutes; stable peak temperature for 120-180 minutes.	Steady increase at 1-2°C per minute in the first 30 minutes, reaching peak temperature at 120-180 minutes.	2-3	(Beyler et al., 2007; Bwalya et al., 2004; Choe et al., 2022; La Scala, 2025; Wang et al., 2024)
2	Hydrocarbon Modified (HC)	Rapid escalation to **1100 °C** within the first 5 minutes; maximum temperature maintained for 15-20 minutes.	Escalates at a rate of 10-20°C per second, achieving peak temperature in just 5 minutes.	0.5-1	(Ping et al., 2023; Spearpoint and Dickson, 2023)such as electric vehicles (EVs
3	Electric Vehicle (EV) Fire	Peaks at **1200 °C**, with localized temperatures exceeding **1500 °C** in battery thermal runaway conditions.	Rapid thermal runaway causes a spike to peak temperature within 3-5 minutes; sustained maximum heat for 10 minutes.	1-2	(Zhou et al., 2026)

of the comparison. The ISO 834 standard fire curve is widely used in building codes and fire resistance tests, where it models a typical building fire with a gradual temperature rise, reaching 1200 °C after several hours. This curve is adequate for predicting the behavior of materials under relatively controlled fire conditions, such as those in residential or commercial buildings.

However, the Hydrocarbon (HC) fire curve, commonly encountered in industrial settings like chemical plants and tunnels, presents a more aggressive scenario. These fires can reach 1100 °C within less of 30 minutes, placing severe thermal stress on materials (Gravit et al., 2018). This rapid escalation leaves little time for materials to dissipate heat, leading to accelerated degradation, especially in concrete and steel structures.

With the rise of electric vehicles (EVs), the EV fire presents another challenge. Fires involving lithium-ion batteries can reach 1200°C quickly and have a prolonged burn time due to the potential for re-ignition ((“(PDF) Modern Vehicle Hazards in Parking Structures and Vehicle Carriers,” 2014) These characteristics make EV fires particularly dangerous in enclosed spaces such as parking garages, where the sustained high temperatures can severely compromise structural integrity.

The ISO 834 fire curve is designed for standard fire tests in building construction and allows for a gradual temperature rise, enabling materials to maintain structural integrity for longer periods. This makes the ISO 834 fire curve suitable for traditional buildings where fire exposure is controlled, with concrete and steel able to absorb the heat before degradation occurs (ISO 834-1, n.d.). However, when applied to more extreme fire scenarios, such as hydrocarbon fires, the limitations of the ISO 834 curve become clear.

Figure 1: Comparison of Fire Curves

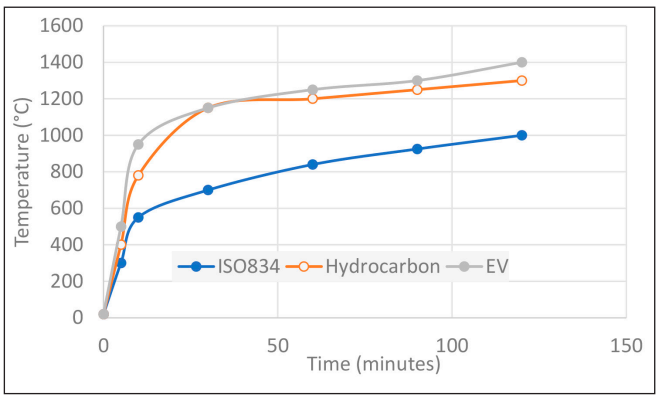

In hydrocarbon fires, particularly in environments like oil refineries and tunnels, the temperature rises much faster. Studies on hydrocarbon fire curves reveal that the Hydrocarbon Modified (HC) fire curve reaches 1100 °C in just a few minutes. This rapid increase causes materials like concrete to experience spalling, where the outer layers of the concrete crack and break away under extreme heat. The rapid loss of compressive strength in concrete and the quick deterioration of steel’s yield strength in such fires make them significantly more dangerous than those modeled by the ISO 834 fire curve (Ali et al., 2009).

For EV fires, which are becoming more frequent due to the rise in electric vehicle adoption, the fire presents even greater challenges. Lithium-ion batteries are prone to thermal runaway, where they reach extreme temperatures within minutes, and once ignited, EV fires can sustain temperatures above 1200 °C, with a risk of re-ignition (Okamoto et al., 2013, 2009) on the right side of the front bumper, or at the seat in the passenger compartment. We observed how the fire spread from the point of origin and investigated the effects of the location of the ignition on the burning behavior. The temperature inside the burning car and the mass loss rate were measured. The burning of a minivan was composed of three compartmental fires: the front compartment (front nose. In parking garages and tunnels, where such fires are more likely to occur, this poses significant risks for the structural stability of buildings (Olenick et al., n.d.).

When comparing the ISO 834, Hydrocarbon, and Electric Vehicle (EV) fires, the differences in temperature-time profiles become apparent in how quickly they impose thermal loads on structural materials. The ISO 834 fire curve models a slow temperature rise, which allows time for structural elements such as concrete and steel to gradually absorb the heat before reaching critical degradation points. This makes the ISO 834 suitable for traditional building fires, where the risk of rapid

Table 2: *Reduction in strength for concrete and steel at various temperatures*

No.	Material	Fire Curve	Temperature (°C)	Strength Reduction (%)	References
1	Concrete	ISO 834	300 °C	10%	(Chen et al., 2024; Kodur, 1999)
2	Concrete	Hydrocarbon Fire	600 °C	50%	(Buchanan and Abu, 2016; Poon et al., 2001)
3	Concrete	EV Fire	800 °C	30%	(Sun et al., 2020b)
4	Concrete	EV Fire	1200 °C	70%	(Sun et al., 2020b)
5	Steel	ISO 834	400 °C	20%	(Ali et al., 2009; Wong et al., 1998)
6	Steel	EV Fire	1000 °C	70%	(Sun et al., 2020b)
7	Steel	Hydrocarbon Fire	700 °C	40%	(Ali et al., 2009; Outinen and Mäkeläinen, 2004)

failure is minimized by the slow escalation of temperature (ISO 834-1, n.d.)

However, the Hydrocarbon fire curve exposes structures to much more intense heat within a short period, resulting in accelerated material degradation. Studies on hydrocarbon fires show that temperatures can reach 1100°C within five minutes, significantly reducing the time available for heat dissipation in materials such as concrete and steel. This leads to more rapid spalling in concrete and a quicker loss of steel's yield strength, which can cause critical structural failures (Morys et al., 2020; Oli et al., 2023).

The EV fire behaves similarly to hydrocarbon fires but presents unique challenges due to the behavior of lithium-ion batteries. These fires not only reach temperatures of 1200 °C but also maintain them for longer durations, with the risk of re-ignition adding to the severity of the fire. The extended exposure to heat makes EV fires particularly dangerous in confined environments like parking garages and tunnels, where prolonged heat can severely weaken reinforced concrete and steel structures (Sun et al., 2020a).

The significant differences between the ISO 834, Hydrocarbon curves, and EV fire are critical for understanding how structures perform under different fire scenarios. The ISO 834 fire curve, with its slow temperature rise, allows materials like concrete and steel to retain their integrity for longer periods. However, the rapid rise in hydrocarbon and EV fires presents much more aggressive thermal conditions.

3. MATERIAL DEGRADATION AND REDUCTION FACTORS

The degradation of structural materials, such as concrete, steel, and composites, under fire conditions depends significantly on the fire's temperature-time profile. Each material behaves differently when exposed to heat, and understanding how they degrade under different fire curves—ISO 834, Hydrocarbon, and EV fires—is critical for ensuring the integrity of structures in fire-prone environments.

Under the ISO 834 fire curve, where temperatures rise gradually over a few hours, concrete typically retains much of its structural integrity for longer periods. At temperatures below 300 °C, concrete's compressive strength remains relatively stable. However, as temperatures approach 600 °C, compressive strength begins to decline significantly, eventually leading to spalling at around 800 °C ("Eurocode 2," n.d.).

In contrast, hydrocarbon fires, with their rapid temperature rise to 1100 °C, induce much faster degradation. Concrete exposed to these high temperatures often suffers from immediate spalling, where the outer layers break away due to rapid thermal expansion. Steel in these conditions loses its yield strength rapidly, particularly when temperatures exceed 500 °C, and composite materials may start to delaminate due to the rapid heat exposure (M. Hedayati et al., 2015).

The EV fire presents a unique challenge, as it combines rapid temperature rise with prolonged exposure to extreme heat. The sustained high temperatures, exceeding 1200°C, lead to a prolonged degradation period, particularly in materials like reinforced concrete, where prolonged heat exposure can weaken the bond between steel reinforcement and concrete, leading to structural instability ("(PDF) Modern Vehicle Hazards in Parking Structures and Vehicle Carriers," 2014)

When exposed to fire, materials such as concrete, steel, and composites undergo significant reductions in strength, stiffness, and overall integrity. The rate and extent of degradation vary depending on the fire curve, with hydrocarbon and EV fires causing more rapid and severe damage than the ISO 834 fire curve. For concrete under hydrocarbon fire events, studies have shown that it begins to lose compressive strength at temperatures above 300 °C, with significant reductions occurring around 600°C and higher. At temperatures above 600 °C, concrete lose their load-bearing capacity, and under extreme conditions like those found in hydrocarbon fires, the rapid heating can cause spalling, where the outer layers of the material crack and break away as presented in *Table 2*. Steel, on the other hand, begins to lose yield strength at around 400 °C, with a 50% reduction at 500 °C (Khoury, 2000).

In electric vehicle (EV) fires, the sustained high temperatures of over 1000 °C can weaken steel to the point where it can no longer support structural loads, leading to buckling and potential collapse. Steel loses around 50% of its strength at temperatures above 600 °C, and prolonged exposure to the extreme heat typical of EV fires accelerates this weakening. One study on EV fires found that jet flames from lithium-ion batteries, combined with combustible materials in the passenger cabin, significantly increased the fire's heat release rate (up to 7.25 MW), threatening adjacent structures in parking garages, including steel and concrete components. These high heat levels promote fire spread and structural risks, especially in enclosed spaces such as parking structures (Kang et al., 2023).

Concrete, while generally resistant to fire, is not immune to damage in EV fire scenarios. The intense heat can cause spalling, where surface layers of the concrete explosively break away due to rapid temperature increases, reducing its

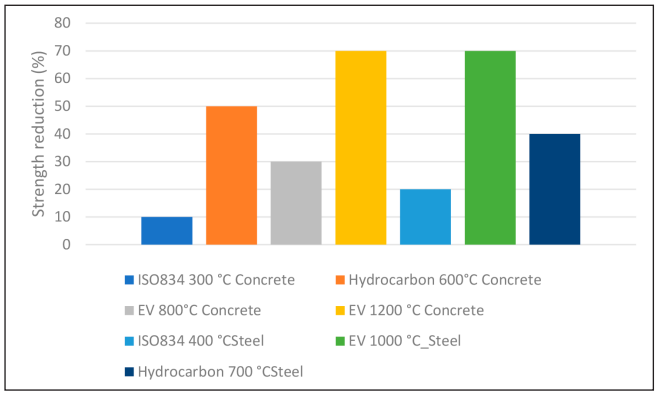

Figure 2: Comparison of Strength Reduction in Concrete and Steel at Various Temperatures

load-bearing capacity and exposing the steel reinforcements to further weakening. Additionally, composites used in modern construction and EV enclosures degrade more rapidly than traditional materials under fire conditions as shown in *Figure 2*. Delamination is a common failure mode for composites in EV fires, where layers of material separate under sustained heat exposure, compromising their structural bonds and accelerating failure (Guerrieri and Fragomeni, 2016). This degradation underscores the need for effective fire suppression systems and heat-resistant materials in parking structures designed for EV use.

As the temperature increases in fire scenarios, the degradation of structural materials becomes more pronounced. In hydrocarbon fires, for example, the rapid rise to 1100 °C not only affects concrete through spalling but also drastically reduces the structural performance of steel and composites. In these scenarios, steel can lose up to 70% of its yield strength within a few minutes, leading to structural failure if the fire persists. This is particularly dangerous in structures like tunnels or industrial facilities, where the high heat from hydrocarbon fires can quickly compromise load-bearing elements (Guerrieri and Fragomeni, 2016).

Under ISO 834 fire conditions, structural materials degrade gradually, allowing more time for elements to absorb and redistribute heat. However, limitations in the ISO 834 fire curve become clear when predicting performance in more severe fire scenarios, such as hydrocarbon and electric vehicle (EV) fires. Studies indicate that while ISO 834 serves as a baseline for fire resistance, hydrocarbon fire conditions reach significantly higher temperatures and cause faster degradation. For example, research shows that the fire resistance rating of Ultra-High Performance Fiber Reinforced Concrete (UHPFRC) beams decreased by 30 minutes under hydrocarbon fires compared to ISO 834, highlighting the inadequacy of ISO 834 in such aggressive conditions (Simwanda et al., 2022). Furthermore, recent analyses recommend adopting custom fire curves beyond ISO 834 for high-risk infrastructure assessments, especially for localized, high-temperature fires from EV or fuel tanker incidents as shown in *Table 3*. This approach supports performance-based fire design, enabling more accurate hazard responses in critical infrastructure (Hu, 2020).

When comparing the degradation of materials under the ISO 834, Hydrocarbon, and Electric Vehicle (EV) fires, the structural impact on concrete, steel, and composite materials becomes more evident. In ISO 834 fire conditions, materials experience slower degradation, with concrete retaining a substantial amount of its compressive strength up to 300 °C. At this temperature, concrete's strength reduction is relatively minor, and steel loses around 20% of its yield strength ("Eurocode 2," n.d.). This gradual degradation allows more time for structural fire resistance measures to mitigate damage, making the ISO 834 fire curve suitable for traditional building fires

However, under hydrocarbon fires, the rapid rise to 1100 °C within just a few minutes causes much more aggressive degradation. Concrete spalling occurs almost immediately, and steel experiences rapid loss of yield strength, reducing by as much as 50% at temperatures above 600 °C. This sudden degradation poses a significant risk to structures like tunnels, industrial facilities, and oil refineries, where fire hazards are more extreme. Without adequate fireproofing, such structures can suffer catastrophic failure in the early stages of a fire(Kumar et al., 2021; Wan et al., 2014).

For EV fires, the sustained exposure to 1200 °C or higher temperatures leads to prolonged degradation of both concrete and steel, as well as composite materials. In enclosed spaces such as parking garages, the continuous heat load can weaken steel reinforcement in concrete, causing spalling and delamination in composite materials. This sustained exposure increases the risk of structural collapse, particularly in locations where fire suppression is delayed, or re-ignition occurs due to the nature of lithium-ion battery fires (Hertz, 2003; ISO 834-1, n.d.; Kodur, 1999).

4. COMPARATIVE ANALYSIS OF FIRE SCENARIOS

In this section, we will focus on comparing the different fire scenarios (ISO 834, Hydrocarbon, and EV fires) in terms of their effects on structural materials, such as concrete, steel, and composites *(Table 4)*. The comparison will include factors like, Temperature-Time Profiles to observe how quickly each fire type reaches peak temperature and sustains it, heat release rates (HRR), in which the rate at which energy is released in the form of heat, crucial for assessing the severity of the fire and reduction Factors, where the extent to which key material properties, like yield strength and compressive strength, are reduced.

When comparing ISO 834, Hydrocarbon, and EV fires as shown in *Table 4 and Figure 3*, it becomes evident that the more severe fire conditions of hydrocarbon and EV fires result in faster material degradation and greater structural challenges. The Heat Release Rate (HRR) is a key factor that distinguishes these fire scenarios. While ISO 834 fires exhibit a slow and gradual rise in HRR, both hydrocarbon and EV fires demonstrate a much more aggressive heat release, which in turn accelerates the degradation of structural materials (Alvares et al., 2016; La Scala et al., 2023).

In hydrocarbon fires, the HRR can reach values as high as 350 kW/m² within 5 minutes, exposing structural materials like steel and concrete to extreme heat and pressure. This rapid escalation results in spalling in concrete and buckling in steel, particularly in tunnels and confined environments. In contrast, ISO 834 fires produce significantly lower HRR, which allows structures more time to resist failure. The prolonged heat exposure seen in EV fires not only increases the HRR but also sustains it at high levels for longer periods. This sustained exposure leads to composite material delamination and prolonged degradation of reinforced concrete, increasing

Table 3: Material Integrity and Time to Failure under Different Fire Scenarios

No.	Fire Curve	Material	Impact on Material Integrity	Time to Failure	References
1	ISO 834 Standard Fire	Concrete	Gradual strength reduction; spalling at temperatures >600°C	2-3 hours	(Kodur, 1999; M. Hedayati et al., 2015; Wang et al., 2024)
2	Hydrocarbon Modified (HC)	Steel	Rapid yield strength loss; structural buckling at >700°C	30-60 minutes	(Ali et al., 2009)
3	Electric Vehicle (EV) Fire	Composites	Delamination; loss of structural bonds under intense heat	1-2 hours	(Kang et al., 2023)

Table 4: Comparative analysis of fire curve

No.	Fire Curve	Peak Temperature (°C)	Time to Peak Temperature (minutes)	Heat Release Rate (kW/m²)	Structural Degradation Speed	References
1	ISO 834 Standard Fire	1000	120-180	100-150	Slow	(Held et al., 2022)
2	Hydrocarbon Fire	1100	5	200-350	Rapid	(Held et al., 2022)
3	Electric Vehicle (EV) Fire	1200	10	250-400	Prolonged	(La Scala, 2025)

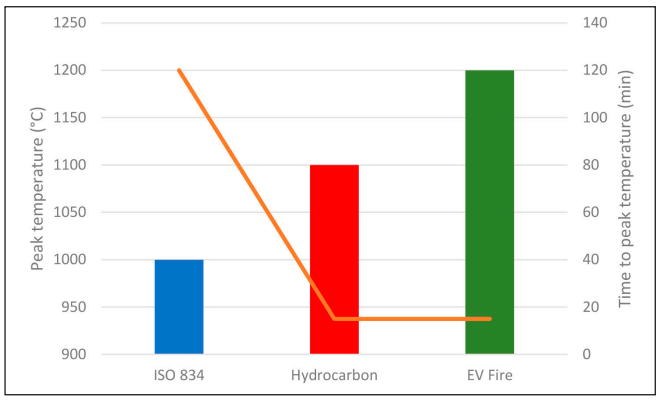

Figure 3: Comparative Analysis of Fire Curves

the likelihood of structural failure in parking garages and tunnels where lithium-ion battery fires are a growing concern (Liu et al., n.d.)

In the comparative analysis of fire scenarios, understanding the temperature-time profiles is critical for assessing how quickly materials reach their failure points. Hydrocarbon fires reach peak temperatures much faster than ISO 834 fires, and EV fires demonstrate an even more sustained high-temperature profile due to the nature of lithium-ion batteries. This creates unique structural challenges, as steel and concrete are exposed to prolonged extreme heat. Under ISO 834 fire conditions, materials like concrete and steel undergo gradual degradation. Concrete typically experiences spalling after a few hours of exposure, and steel retains up to 50% of its yield strength at 600 °C. However, hydrocarbon fires reduce this timeframe dramatically, with temperatures reaching 1100 °C in less than 5 minutes. The rapid rise in temperature causes steel to buckle and concrete to spall almost immediately, posing a significant risk in industrial facilities and tunnels (Oli et al., 2023).

In EV fires, the prolonged exposure to 1200 °C creates even more severe conditions. The thermal runaway effect not only results in rapid temperature rise but also sustained heat exposure. This leads to more significant structural challenges in parking garages and tunnels, where prolonged exposure to high heat weakens reinforced concrete and causes delamination in composite materials (Chen et al., 2021)

The next graph will visually compare the temperature-time profiles for ISO 834, Hydrocarbon, and EV fires, showing the steep rise in temperature for hydrocarbon and EV fires compared to the gradual rise in ISO 834.

The final part of the Comparative Analysis focuses on the structural responses to these varying fire scenarios. Each fire type - ISO 834, Hydrocarbon, and EV fires - affects structural materials differently based on how quickly the fire escalates and how long it sustains extreme temperatures. These factors play a crucial role in determining how structures such as parking garages, tunnels, and industrial buildings withstand fires and what measures are required to prevent catastrophic failure.

In ISO 834 fires, which simulate typical building fires, reinforced concrete and steel perform better due to the slow temperature rise. The gradual heating allows the structure to resist collapse for longer, often giving enough time for fire suppression or evacuation (ISO 834-2, 2019). However, hydrocarbon fires and EV fires expose materials to far greater thermal stresses in much shorter periods. Concrete undergoes rapid spalling in both fire types, which compromises its compressive strength. Steel suffers from buckling and yield strength loss under hydrocarbon and EV fire conditions, particularly in confined spaces like tunnels and parking garages (Ariyanayagam and Mahendran, n.d.).

In EV fires, the sustained exposure to high temperatures poses a unique threat, as the thermal runaway from lithium-ion batteries can cause multiple reignition events, further weakening the structural integrity of both concrete and steel. Composite materials used in modern construction also degrade faster under these conditions, with delamination occurring as the adhesive bonds fail at high temperatures (Mellert et al., 2018).

5. CONCLUSION

This study provides a comprehensive comparison of the ISO 834, Hydrocarbon (HC), and Electric Vehicle (EV) fire

curves, emphasizing their impacts on structural materials such as concrete, steel, and composites. The findings demonstrate that while the ISO 834 fire curve remains effective for moderate-risk scenarios, such as those in residential and commercial buildings, it fails to account for the aggressive nature of HC and EV fires. These fires are characterized by rapid temperature escalation and prolonged high-temperature exposure, which impose severe thermal loads on structures. Moreover, due to the notable similarities between HC and EV fire behaviors, the HC fire curve can serve as a basis for evaluating EV fires, enabling a practical approach for assessing their effects on concrete structures.

The traditional ISO 834 fire curve is suitable for typical building fire scenarios where the gradual temperature increase allows materials like steel and concrete to maintain their integrity for longer periods. However, in environments exposed to extreme fire scenarios, such as tunnels, industrial facilities, and parking garages, the limitations of this curve become apparent. Hydrocarbon fires, with temperatures reaching 1100 °C in under five minutes, cause rapid structural degradation, including concrete spalling and significant reductions in steel strength, increasing the likelihood of structural collapse. EV fires, on the other hand, pose unique challenges due to thermal runaway in lithium-ion batteries, which leads to sustained temperatures exceeding 1200 °C. This prolonged exposure weakens reinforced concrete and delaminates composite materials, significantly heightening the risk of failure, particularly in confined spaces such as parking garages.

Adapting the HC fire curve for EV fire evaluation provides a valuable framework for addressing these risks. By leveraging the thermal similarity between HC and EV fires, it becomes feasible to streamline safety assessments and design measures for structures exposed to these fire types. Enhanced fireproofing strategies, including fire-resistant coatings for steel and heat-resistant additives for concrete, are essential to mitigate the rapid degradation caused by HC and EV fires. Additionally, advanced ventilation systems and fire suppression technologies must be incorporated into structural designs to manage the unique risks posed by these fire scenarios.

The need for updated fire safety standards and building codes is clear. Existing standards, primarily designed around ISO 834 fire scenarios, must evolve to incorporate the thermal and structural demands of HC and EV fires. Revising these codes to mandate the use of fire-resistant materials and the implementation of thermal modeling for high-risk environments will ensure greater safety and resilience. Recognizing the parallels between HC and EV fires and adapting HC fire evaluations for EV-specific scenarios offer a cost-effective approach to improving fire safety while maintaining robust structural performance. This study underscores the importance of addressing modern fire hazards through enhanced materials, updated codes, and innovative design adaptations, ensuring safer and more resilient structures capable of withstanding the challenges of contemporary fire risks.

6. REFERENCES

Ali, F., Nadjai, A., Abu-Tair, A., 2009. Experimental and Numerical Study on Performance of Concrete Slabs Subjected to Severe Fire. Fire Safety Science 9, 1255–1266. https://doi.org/10.3801/IAFSS.FSS.9-1255

Alvares, N., Hasegawa, H., Staggs, K., 2016. Ignition, Heat Release Rate and Suppression of Elastomeric Materials. Fire Technol 52, 1575–1593. https://doi.org/10.1007/s10694-015-0483-0

Ariyanayagam, A.D., Mahendran, M., n.d. Fire Safety of Buildings Based on Realistic Fire Time-Temperature Curves.

Beyler, C., Beitel, J., Iwankiw, N., Lattimer, B., 2007. Fire Resistance Testing for Performance-based Fire Design of Buildings. Final Report.

Buchanan, A.H., Abu, A.K., 2016. Structural Design for Fire Safety, 1st ed. Wiley. https://doi.org/10.1002/9781118700402

Bwalya, A., Sultan, M., Benichou, N., 2004. Design fires for fire safety engineering: a state-of-the-art review.

Caner, A., Zlatanic, S., Munfah, N., 2005. Structural Fire Performance of Concrete and Shotcrete Tunnel Liners. J. Struct. Eng. 131, 1920–1925. https://doi.org/10.1061/(ASCE)0733-9445(2005)131:12(1920)

Chen, J., Xiong, P., Li, K., Yang, S., 2024. Optimization Study of Fire Prevention Structure of Electric Vehicle Based on Bottom Crash Protection. Fire 7, 209. https://doi.org/10.3390/fire7070209

Chen, Y., Kang, Y., Zhao, Y., Wang, L., Liu, J., Li, Y., Liang, Z., He, X., Li, X., Tavajohi, N., Li, B., 2021. A review of lithium-ion battery safety concerns: The issues, strategies, and testing standards. Journal of Energy Chemistry 59, 83–99. https://doi.org/10.1016/j.jechem.2020.10.017

Choe, L., Ramesh, S., Dai, X., Hoehler, M., Bundy, M., 2022. Experimental study on fire resistance of a full-scale composite floor assembly in a two-story steel framed building. JSFE 13, 145–161. https://doi.org/10.1108/JSFE-05-2021-0030

Eurocode 2: Structural Fire Design 2023 | PDF | Strength Of Materials | Beam (Structure) [WWW Document], n.d. . Scribd. URL https://www.scribd.com/document/903414681/BS-EN-1992-1-2-2023-2025-08-19-05-09-21-AM (accessed 3.30.26).

Gravit, M., Gumerova, E., Bardin, A., Lukinov, V., 2018. Increase of Fire Resistance Limits of Building Structures of Oil-and-Gas Complex Under Hydrocarbon Fire, in: Murgul, V., Popovic, Z. (Eds.), International Scientific Conference Energy Management of Municipal Transportation Facilities and Transport EMMFT 2017, Advances in Intelligent Systems and Computing. Springer International Publishing, Cham, pp. 818–829. https://doi.org/10.1007/978-3-319-70987-1_87

Guerrieri, M., Fragomeni, S., 2016. Mechanisms of Spalling of Concrete Panels of Different Geometry in Hydrocarbon Fire. J. Mater. Civ. Eng. 28, 04016164. https://doi.org/10.1061/(ASCE)MT.1943-5533.0001680

Held, M., Tuchschmid, M., Zennegg, M., Figi, R., Schreiner, C., Mellert, L.D., Welte, U., Kompatscher, M., Hermann, M., Nachef, L., 2022. Thermal runaway and fire of electric vehicle lithium-ion battery and contamination of infrastructure facility. Renewable and Sustainable Energy Reviews 165, 112474. https://doi.org/10.1016/j.rser.2022.112474

Hertz, K.D., 2003. Limits of spalling of fire-exposed concrete. Fire Safety Journal 38, 103–116. https://doi.org/10.1016/S0379-7112(02)00051-6

Hu, J., 2020. Highway bridges in fire: characterisation of fire loading and structural behaviour.

ISO 834-1, n.d. Fire-resistance tests—Elements of building construction—General requirements, 1999th ed.

Kang, S., Kwon, M., Yoon Choi, J., Choi, S., 2023. Full-scale fire testing of battery electric vehicles. Applied Energy 332, 120497. https://doi.org/10.1016/j.apenergy.2022.120497

Khoury, G.A., 2000. Effect of fire on concrete and concrete structures. Progress Structural Eng Maths 2, 429–447. https://doi.org/10.1002/pse.51

Kodur, V.K.R., 1999. Fire performance of high-strength concrete structural members. Construction Technology Update 31. https://doi.org/10.4224/40002842

Kumar, W., Sharma, U.K., Shome, M., 2021. Mechanical properties of conventional structural steel and fire-resistant steel at elevated temperatures. Journal of Constructional Steel Research 181, 106615. https://doi.org/10.1016/j.jcsr.2021.106615

La Scala, A., 2025. Experimental and numerical investigation of vibrations induced by manual demolition work in masonry buildings. Sci Rep 16, 1500. https://doi.org/10.1038/s41598-025-31057-3

La Scala, A., Loprieno, P., Foti, D., La Scala, M., 2023. The Mechanical Response of Structural Elements in Enclosed

Structures during Electric Vehicle Fires: A Computational Study. Energies 16, 7233. https://doi.org/10.3390/en16217233
Liu, Y., Cassady, S., Jones, E., Pospisil, P., n.d. Review of Design Fire Heat Release Rate for Tunnels with Fire Suppression Systems.
M. Hedayati, M. Sofi, Mendis, P., Ngo, T., 2015. A Comprehensive Review of Spalling and Fire Performance of Concrete Members. EJSE 15, 8–34. https://doi.org/10.56748/ejse.15199
Mellert, L.D., Welte, U., Hermann, M., Kompatscher, M., Ponticq, X., Hagerbach, V., 2018. ELECTRIC MOBILITY AND ROAD TUNNEL SAFETY HAZARDS OF ELECTRIC VEHICLE FIRES.
Morys, M., Häßler, D., Krüger, S., Schartel, B., Hothan, S., 2020. Beyond the standard time-temperature curve: Assessment of intumescent coatings under standard and deviant temperature curves. Fire Safety Journal 112, 102951. https://doi.org/10.1016/j.firesaf.2020.102951
Nguyen, T.N.A., Lai, H.-T., Fernandes, R., Dall'Olio, F.G., Blériot, C., Ha-Duong, T., Brenner, C., 2025. Apoptosis-inducing factor (AIF) at the crossroad of cell survival and cell death: implications for cancer and mitochondrial diseases. Cell Commun Signal 23, 264. https://doi.org/10.1186/s12964-025-02272-2
Okamoto, K., Otake, T., Miyamoto, H., Honma, M., Watanabe, N., 2013. Burning behavior of minivan passenger cars. Fire Safety Journal 62, 272–280. https://doi.org/10.1016/j.firesaf.2013.09.010
Okamoto, K., Watanabe, N., Hagimoto, Y., Chigira, T., Masano, R., Miura, H., Ochiai, S., Satoh, H., Tamura, Y., Hayano, K., Maeda, Y., Suzuki, J., 2009. Burning behavior of sedan passenger cars. Fire Safety Journal 44, 301–310. https://doi.org/10.1016/j.firesaf.2008.07.001
Olenick, S., Klassen, M., Hussain, N., n.d. Classification of Modern Vehicle Hazards in Parking Structures & Systems – Ph II.
Oli, T., Ha, D., Jang, T., Park, C., Kim, G., Kim, S., 2023. Temperature Distribution Curve Analysis on Concrete through LS-DYNA. Fire 7, 15. https://doi.org/10.3390/fire7010015
Outinen, J., Mäkeläinen, P., 2004. Mechanical properties of structural steel at elevated temperatures and after cooling down. Fire and Materials 28, 237–251. https://doi.org/10.1002/fam.849
(PDF) Modern Vehicle Hazards in Parking Structures and Vehicle Carriers [WWW Document], 2014. . ResearchGate. URL https://www.researchgate.net/publication/343344348_Modern_Vehicle_Hazards_in_Parking_Structures_and_Vehicle_Carriers#fullTextFileContent (accessed 3.30.26).
Ping, P., Dai, X., Kong, D., Zhang, Y., Zhao, H., Gao, X., Gao, W., 2023. Experimental study on nano-encapsulated inorganic phase change material for lithium-ion battery thermal management and thermal runaway suppression. Chemical Engineering Journal 463, 142401. https://doi.org/10.1016/j.cej.2023.142401
Poon, C.-S., Azhar, S., Anson, M., Wong, Y.-L., 2001. Comparison of the strength and durability performance of normal- and high-strength pozzolanic concretes at elevated temperatures. Cement and Concrete Research 31, 1291–1300. https://doi.org/10.1016/S0008-8846(01)00580-4
Simwanda, L., Kahanji, C., Ali, F., 2022. Numerical modelling, parametric analysis and design of UHPFRC beams exposed to fire. https://doi.org/10.21203/rs.3.rs-1582849/v1
Spearpoint, M., Dickson, S., 2023. An overview of the impacts of autonomous vehicles on fire safety in parking buildings. Proceedings of the Institution of Civil Engineers - Transport 176, 142–152. https://doi.org/10.1680/jtran.22.00028
Sun, P., Bisschop, R., Niu, H., Huang, X., 2020a. A Review of Battery Fires in Electric Vehicles. Fire Technol 56, 1361–1410. https://doi.org/10.1007/s10694-019-00944-3
Sun, P., Bisschop, R., Niu, H., Huang, X., 2020b. A Review of Battery Fires in Electric Vehicles. Fire Technol 56, 1361–1410. https://doi.org/10.1007/s10694-019-00944-3
Wan, R., Sun, F., Zhang, L., Shan, A., 2014. Effect of Mo Addition on Strength of Fire-Resistant Steel at Elevated Temperature. J. of Materi Eng and Perform 23, 2780–2786. https://doi.org/10.1007/s11665-014-1051-3
Wang, Y., Liu, Z., Zhang, X., Qu, S., Xu, T., 2024. Fire resistance of reinforced concrete columns: State of the art, analysis and prediction. Journal of Building Engineering 96, 110690. https://doi.org/10.1016/j.jobe.2024.110690
Wong, M.B., Ghojel, J.I., Crozier, D.A., 1998. Temperature-time analysis for steel structures under fire conditions. Structural Engineering and Mechanics 6, 275–289. https://doi.org/10.12989/sem.1998.6.3.275
Zhao, Y., Kong, J., Cao, Y., Liu, H., You, W., 2025. Mapping the Evolution of New Energy Vehicle Fire Risk Research: A Comprehensive Bibliometric Analysis. Fire 8, 395. https://doi.org/10.3390/fire8100395
Zhou, Z., Yang, W., Yan, Z., Zhu, H., Shen, Y., 2026. Impact of fire on the transverse and longitudinal structural mechanical behavior of deep-buried large-diameter dual-layer lining tunnels. Tunnelling and Underground Space Technology 167, 106987. https://doi.org/10.1016/j.tust.2025.106987

Bara Alseid is a civil engineer specializing in structural and concrete engineering, with a focus on the behaviour and design of reinforced concrete structures. His work involves the analysis of structural performance under mechanical loading, fire exposure, and durability-related conditions.

Éva Lublóy is a full professor at the Budapest University of Technology and Economics, specializing in concrete and reinforced concrete structures. Her research focuses on the fire performance of concrete, the temperaturedependent behaviour of structural materials, and the optimization of concrete mixtures for improved durability and sustainability.

ENHANCING CONCRETE STRENGTH MONITORING VIA DEEP LEARNING FUSION OF NON-DESTRUCTIVE TESTING DATA

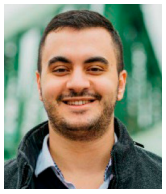

Hatem Affes - Salem G. Nehme - Béla Paláncz †

https://doi.org/10.32970/CS.2025.1.3

Accurate monitoring of concrete strength evolution is critical for construction safety and timeline optimization. Traditional Non-Destructive Testing (NDT) methods, such as Ultrasonic Pulse Velocity (UPV) or Rebound Hammer, often suffer from low accuracy when used in isolation due to the influence of aggregate types and moisture content. This study employs a Self-Normalizing Neural Network (SNN) to fuse multi-sensor NDT data for predicting compressive strength. The model utilizes a dataset of 4,420 monitoring points from concrete mixtures containing various aggregate types (including recycled and volcanic) and additives. The input variables include Curing Age, Ultrasonic Pulse Velocity (UPV), and Electrical Resistivity, while the output is Compressive Strength. Results indicate that the Deep Learning fusion model significantly outperforms traditional regression curves, achieving high accuracy (> 0.90) by effectively capturing the non-linear relationships between NDT metrics and strength development. This approach offers a non-invasive, sustainable method for verifying structural integrity in aggressive environments . Crucially the analysis identifies a specific "High Risk Zone" where concrete exhibits adequate structural strength (>30 MPa) but critically low electrical resistivity. This discrepancy highlights a matrix that is mechanically sound yet highly permeable to ionic ingress, identifying vulnerabilities to acid attack that standard strength testing would miss. These findings validate the SNN framework as a dual-objective monitoring tool for ensuring the resilience of wastewater infrastructure.

Keywords: Concrete compressive strength; Machine Learning; Deep Learning; Self-Normalizing Networks; Quality Control

1. INTRODUCTION

The compressive strength of concrete is fundamentally governed by its internal matrix, specifically the quality of the cement paste, aggregate interlock, and the water-to-cement ratio. While optimizing these mix parameters is essential for achieving theoretical load-bearing capacity, infrastructure operating in aggressive environments; particularly wastewater facilities; faces simultaneous mechanical and chemical threats that cannot be predicted by mix design alone. External stressors such as sulfate attack, chloride ingress, and freeze-thaw cycles degrade the matrix over time, causing microstructural damage that compromises structural integrity. Consequently, relying solely on initial design assumptions or destructive coring is impractical for long-term safety. Continuous, non-invasive monitoring is therefore critical to track the evolution of strength and verify resilience against chemical degradation.

The compressive strength largely depends on the concrete matrix. Several parameters *(Figure 1)* influence the compressive strength, including the water-to-cement ratio, the type and quality of cement and aggregates, and the presence of admixtures. A lower w/c ratio results in a denser and less porous matrix *(Figure 2),* leading to higher strength. Conversely, a higher w/c ratio increases porosity and reduces

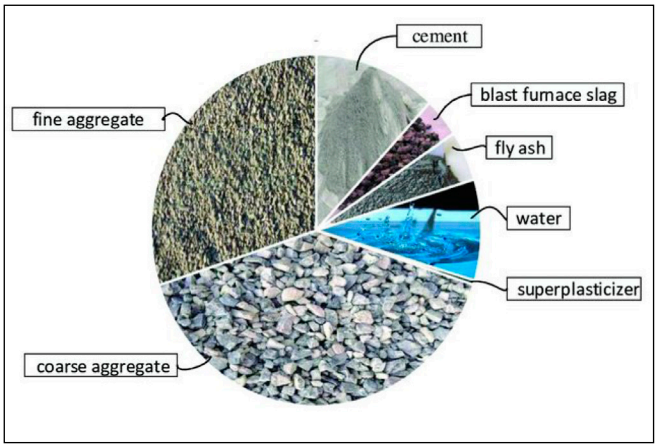

Figure 1: Concrete composition (Yuan Chen et al).

strength. (Neville, 2011) highlights that an optimal w/c ratio is essential for achieving the desired strength without compromising workability.

The type of cement used can influence the rate of hydration and the development of strength. High-strength cement, such as Portland cement, tends to provide better early-age and long-term strength. The quality of the cement, including its fineness and chemical composition, also plays a role (P. Kumar Mehta & Paulo J. M. Monteiro., 2014).

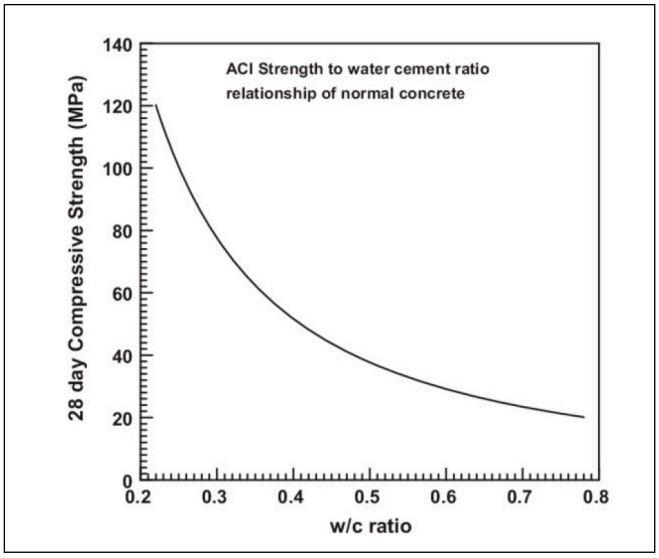

Figure 2: Strength to water-cement ratio relationship of conventional concrete (ACI).

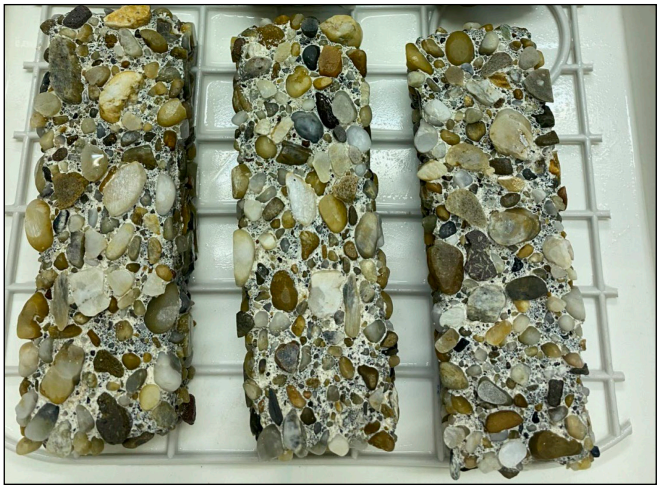

Figure 3: Chemical Attack on Concrete: Image depicting the effects of a 5% sulphuric acid attack, with brushing, on concrete specimens. CEMI 0.5% w/c 330kg after 4 weeks.

The size, shape, and grading of aggregates affect the concrete's strength. Well-graded aggregates with a variety of sizes fill the voids more effectively, enhancing the matrix's density and strength. Additionally, the bond between the cement paste and the aggregates is crucial; rough-textured aggregates typically form stronger bonds compared to smooth-textured ones (S. Mindess et al., 2003). Admixtures can enhance the strength by improving the matrix's microstructure. Superplasticizers, fly ash, and silica fume can significantly enhance compressive strength by improving workability and modifying the microstructure of the cement paste. These additives help reduce the w/c ratio without compromising workability and contribute to the formation of a denser, more durable matrix (ACI, 2008). Proper curing is vital for the hydration of cement and the development of strength. Maintaining adequate moisture and temperature conditions ensures that the chemical reactions proceed to completion, leading to a more robust matrix. Improper curing can lead to incomplete hydration and reduced strength.

Environmental factors such as exposure to aggressive chemicals, freeze-thaw cycles, and high temperatures can cause degradation. Concrete is susceptible to chemical degradation *(Figure 3)* from exposure to aggressive substances such as sulfates and chlorides. Sulfate attack can lead to the formation of expansive products like ettringite, causing cracking and spalling. Chlorides, often from deicing salts or seawater, can penetrate the concrete and cause corrosion of embedded steel reinforcement, leading to structural weakening (Neville, 2011).

Physical stresses like freeze-thaw cycles can cause cracking and spalling, reducing overall compressive strength. In regions with fluctuating temperatures, concrete can be subjected to freeze-thaw cycles. Water trapped in concrete pores expands upon freezing, leading to internal stresses, cracking, and eventual spalling. Using air-entraining agents can mitigate this damage by creating small air bubbles that provide space for the expanding water (S. Mindess et al., 2003). Elevated temperatures can accelerate the hydration process initially but may lead to reduced long-term strength due to forming a less dense microstructure. Prolonged exposure to high temperatures can also cause thermal cracking and degradation of the cement paste. (P. Kumar Mehta & Paulo J. M. Monteiro., 2014). Concrete can be attacked by acidic environments, which dissolve the calcium hydroxide in the cement paste and lead to the formation of soluble products. This attack can severely compromise the strength and integrity of the concrete, especially in industrial environments where acids are prevalent *(Figure 4)*.

Understanding the factors that influence the compressive strength of concrete and the mechanisms that can lead to its degradation is essential for designing durable and resilient structures. While various strategies can enhance the strength, such as optimizing the water-to-cement ratio, using high-quality materials, and incorporating admixtures, it is equally important to consider environmental exposure

Figure 4: Typical failure characteristics of concrete specimens under different freeze-thaw cycles (Zhang et al., 2021)

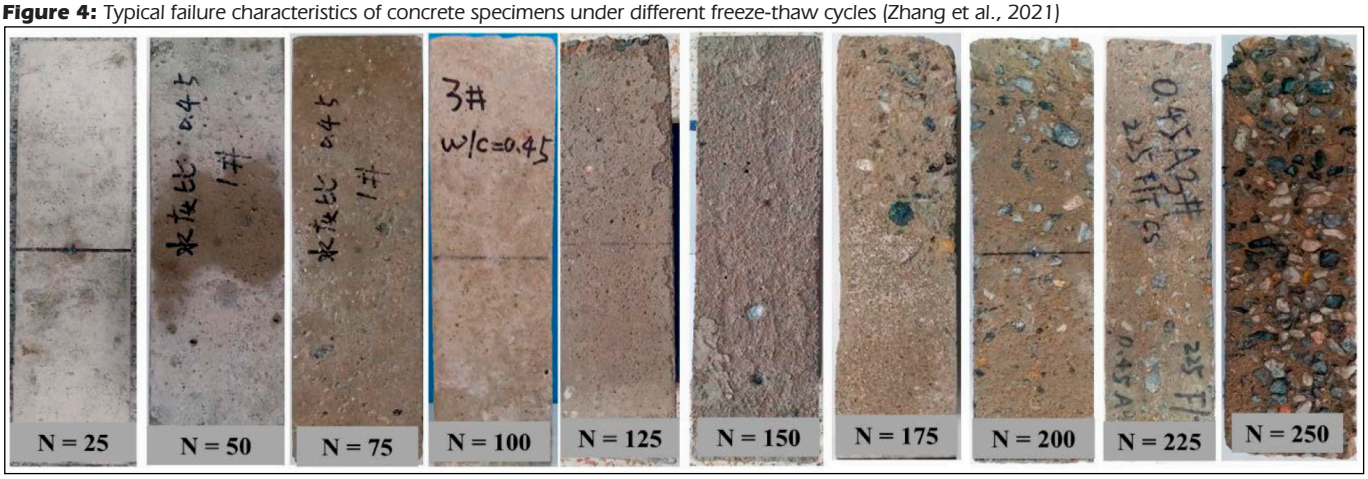

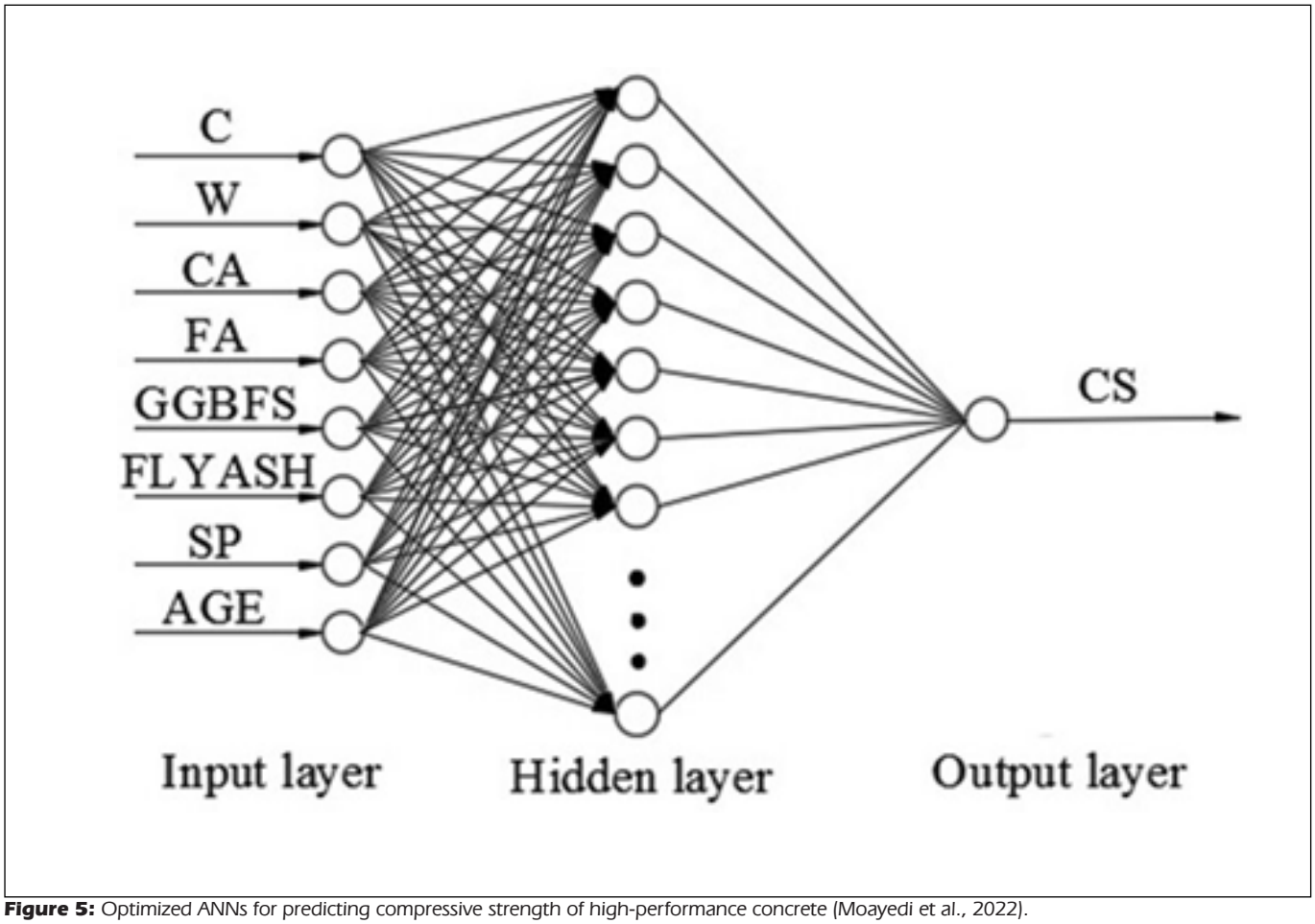

Figure 5: *Optimized ANNs for predicting compressive strength of high-performance concrete (Moayedi et al., 2022).*

and implement measures to protect the concrete from chemical attacks, freeze-thaw cycles, and high temperatures. Traditionally, this prediction has relied on empirical methods and experience-based heuristics. However, these methods can be time-consuming and may not always capture the complex relationships between the various components of concrete. As such, there is growing interest in using artificial intelligence (AI) to enhance the accuracy and efficiency of these predictions.

The process of utilizing AI for predicting concrete compressive strength involves several steps: data collection and preprocessing, model development, and model validation and testing. The dataset typically includes features like cement content, blast furnace slag, fly ash, water content, superplasticizer, coarse aggregate, fine aggregate, and the age of the concrete, with the output being the compressive strength. During model development, the data is split into training and test sets, scaled and normalized, appropriate AI algorithms are selected and tuned, and the models are trained and evaluated using metrics such as mean squared error (MSE) or root mean squared error (RMSE). Finally, the models are validated on a separate test set to ensure they generalize well, avoiding overfitting, where the model performs well on training data but poorly on new data.

AI techniques, including machine learning (ML) and deep learning (DL), have shown promise in predicting the compressive strength of concrete. AI applications in this domain focus on developing models that can predict concrete compressive strength based on various input parameters. Future research could integrate AI with advanced technologies like the Internet of Things (IoT) and Building Information Modeling (BIM) to create comprehensive predictive models. AI models can significantly reduce the time and cost associated with traditional testing methods. Moreover, they can provide real-time predictions, aiding in faster decision-making during the construction process.

Artificial Neural Networks (ANNs) *(Figure 5)* are inspired by the human brain and consist of interconnected layers of nodes, or neurons. These networks are particularly adept at handling nonlinear problems, making them ideal for predicting concrete compressive strength where input variables exhibit complex relationships. ANNs learn from data by adjusting the weights of connections between neurons through a process called training. This allows them to model sophisticated patterns and interactions in the data. A study by Siddique et al. (2021) demonstrated that ANNs could accurately predict concrete compressive strength using input parameters such as cement, sand, coarse aggregate, fly ash as partial replacement of cement, bottom ash as partial replacement of sand, water and water/powder ratio, superplasticizer dosage.

Despite the need for continuous monitoring, traditional Non-Destructive Testing (NDT) methods, such as Ultrasonic Pulse Velocity (UPV) or Rebound Hammer, often suffer from low accuracy when used in isolation due to the confounding influence of aggregate types and moisture content. Furthermore, conventional empirical regression models fail to capture the complex, non-linear relationships between these NDT metrics and the concrete's internal hardening process.

To address this gap, recent advancements in Artificial Intelligence (AI) offer a robust pathway for fusing multi-sensor data. While standard machine learning models like Random Forests and Support Vector Machines have shown promise, Deep Learning architectures provide superior capabilities for modeling high-level abstractions in large,

multivariate datasets. This study employs a Self-Normalizing Neural Network (SNN) to fuse NDT data for predicting compressive strength. By integrating Ultrasonic Pulse Velocity (UPV) with Electrical Resistivity (E_r); a parameter inversely proportional to ion diffusivity; the proposed model aims to create a unified monitoring framework. This approach not only predicts mechanical load capacity with high accuracy (>0.90) but also simultaneously tracks the concrete's resistance to chemical ingress, offering a sustainable solution for quality control in aggressive wastewater environments.

2. MATERIALS AND METHODS

2.1. Dataset Description

The study utilizes the 'ConcreteXAI' dataset, a comprehensive multivariate repository for concrete monitoring. The dataset comprises 4,420 data points derived from 12 distinct concrete mixtures. These mixtures incorporate four types of cement (e.g., CPO 30R, CPC 40R), four types of aggregates (Crushed, Rounded, Recycled, and Volcanic), and various additives including blast furnace slag and Opuntia ficus indica mucilage. As a brief context, in Mexico and parts of South America, this mucilage was added to lime mortar and stucco. It acts as a binding agent and makes the plaster more water-resistant and durable. Some restoration projects still use "cactus slime" to repair historical adobe buildings. The data captures the temporal evolution of mechanical properties, with measurements taken at 3, 7, 14, 28, 40, 60, 90, and 120 days.

While direct chemical degradation data was not available, a Chemical Resistance Potential (CRP) index was computationally derived from the water-to-binder ratio and binder density, following the durability principles of EN 206, to assess the theoretical longevity of the mixtures.

Unlike traditional mix-design prediction models, this study focuses on non-destructive monitoring. The input vector (X) for the Machine Learning model consists of five key variables:

1. Curing Age (days): Temporal factor representing hydration progress.
2. Ultrasonic Pulse Velocity (m/s): An NDT metric correlating with concrete density and elastic modulus.
3. Electrical Resistivity (Ω/cm): An NDT metric correlating with pore structure and permeability.
4. Cement Type: Categorical variable encoding the binder class.
5. Aggregate Type: Categorical variable accounting for the varying density and stiffness of recycled vs. natural aggregates.

The primary output variable (Y) is the Compressive Strength (MPa).

2.2. Computational Framework

Data preprocessing and model training were performed using Wolfram Mathematica. The raw data was normalized to the range [-1, 1] to prevent features with larger magnitudes (such as UPV in m/s) from dominating the learning gradients compared to smaller features (such as Curing Age). The dataset was randomly partitioned into a training set (90%) and a validation set (10%). Due to the large volume of data (N=4,420), the 10% validation set comprises 442 samples; a quantity that exceeds the total dataset size of many comparable studies in this domain. This ensures statistical rigor while allowing the SNN to leverage nearly 4,000 samples to map the complex, non-linear dependencies of the diverse aggregate mixtures

While the primary objective is monitoring compressive strength, the study integrates durability assessment through the analysis of Electrical Resistivity (E_r). In the context of wastewater infrastructure, concrete durability is governed by permeability and the resistance to ionic ingress (e.g., sulfates and chlorides).Instead of relying on theoretical indices based on mix design assumptions, this study utilizes the measured Electrical Resistivity as a direct physical proxy for durability. According to the Nernst-Einstein relationship, resistivity is inversely proportional to the diffusivity of ions within the pore network. Therefore, by including in the input vector, the machine learning model implicitly learns the relationship between the microstructural refinement (durability) and the mechanical load capacity (strength), allowing for a holistic assessment of the concrete's condition.

2.3. Machine Learning Models

We evaluated four distinct algorithms to determine the optimal approach for fusing the NDT sensor data:

- k-Nearest Neighbors (k-NN): Utilized as a non-parametric baseline, this method predicts compressive strength based on the local similarity of NDT vectors in the feature space. It assumes that concrete samples with similar UPV and Resistivity values will exhibit similar strength, serving as a control to test if the problem requires complex non-linear modeling.
- Random Forest (RF): An ensemble learning method that constructs multiple decision trees during training. RF was selected for its robustness in handling categorical variables (e.g., Aggregate Types) and its resistance to overfitting compared to single decision trees. It serves as the primary "shallow" learning benchmark.
- Artificial Neural Networks (ANN): A standard feed-forward Multi-Layer Perceptron (MLP) used to benchmark Deep Learning performance.
- Self-Normalizing Neural Networks (SNN): The proposed deep learning architecture. Unlike standard ANNs which often suffer from vanishing gradients as depth increases, SNNs employ Scaled Exponential Linear Units (SELU) to induce self-normalizing properties. This allows for the stable training of deeper networks, enabling the model to

Table 1: Comparison of Model Performance

Model	RMSE (MPa)	R^2
Nearest Neighbors	3.21	0.94
Random Forest	4.05	0.89
SNN Deep Learning	2.98	0.96

capture high-order, non-linear interactions between the physical NDT metrics (UPV, resistivity) and the chemical properties of the diverse aggregate mixtures.

3. RESULTS ANALYSIS

3.1. Model Performance

The predictive accuracy of the models was evaluated using Root Mean Square Error (RMSE) and the Coefficient of Determination (R^2). As shown in Table 1, the Deep Learning (SNN) model outperformed traditional ML methods.

3.2. Error Analysis

Figure 6 illustrates the distribution of prediction errors. The SNN model shows tight clustering around zero, with 92% of predictions falling within the ±5 MPa tolerance required for industrial quality control. The model performed most accurately in the 30–50 MPa range. This interval corresponds to standard structural concrete classes (e.g., C30/37) widely used in European construction, including Hungary. This high precision in the "structural zone" validates the proposed NDT fusion method as a reliable alternative to destructive coring for supporting compliance with Eurocode 2 standards.

3.3. Prediction of Chemical Degradation Resistance

The study extended the machine learning analysis to evaluate the relationship between compressive strength and resistance to chemical degradation. Although high compressive strength is often correlated with low permeability, optimizing solely for strength does not guarantee durability in aggressive environments (e.g., acidic or sulfate-rich sewage typical of industrial zones).

Figure 7 illustrates the correlation between the predicted compressive strength and the measured Electrical Resistivity (E_r). The analysis reveals a positive correlation (R ≈ 0.68), confirming that the SNN model effectively identifies concrete states that possess a dense microstructure capable of resisting chemical ingress.

However, the model identified specific "high-risk" clusters where adequate compressive strength (>30 MPa) was achieved, but Electrical Resistivity remained low (<5 kΩ/cm). This discrepancy indicates a matrix that is mechanically sound but potentially porous, increasing susceptibility to acid attack and chloride infiltration[1].

By integrating the Electrical Resistivity input, the proposed SNN model functions as a dual-objective monitoring tool. It verifies that the concrete satisfies mechanical requirements (according to MSZ 4798-1) while simultaneously ensuring the resistivity threshold required for long service life in aggressive wastewater environments is met.

4. LIMITATIONS OF THE STUDY

While the proposed Self-Normalizing Neural Network (SNN) demonstrates high predictive accuracy (R^2 > 0.90) within the validation set, three key limitations must be acknowledged for practical implementation in wastewater infrastructure:

- Sensitivity to Moisture Content: The model relies heavily on Electrical Resistivity as a predictor. However, resistivity measurements are highly sensitive to the concrete's saturation degree. Since the training data reflects controlled laboratory curing conditions (likely saturated or sealed), the model's reliability may fluctuate in real-world sewage pipes where moisture levels vary due to fluctuating effluent levels. Future iterations must incorporate a "moisture correction factor" to standardize field readings.
- Regional Aggregate Calibration: The SNN was trained on the ConcreteXAI dataset, which utilizes specific aggregate types (Recycled, Volcanic, Crushed) sourced from North America (Mexico). While the model generalizes well across these categories, applying it to Central European

Figure 6: Relative error of the output

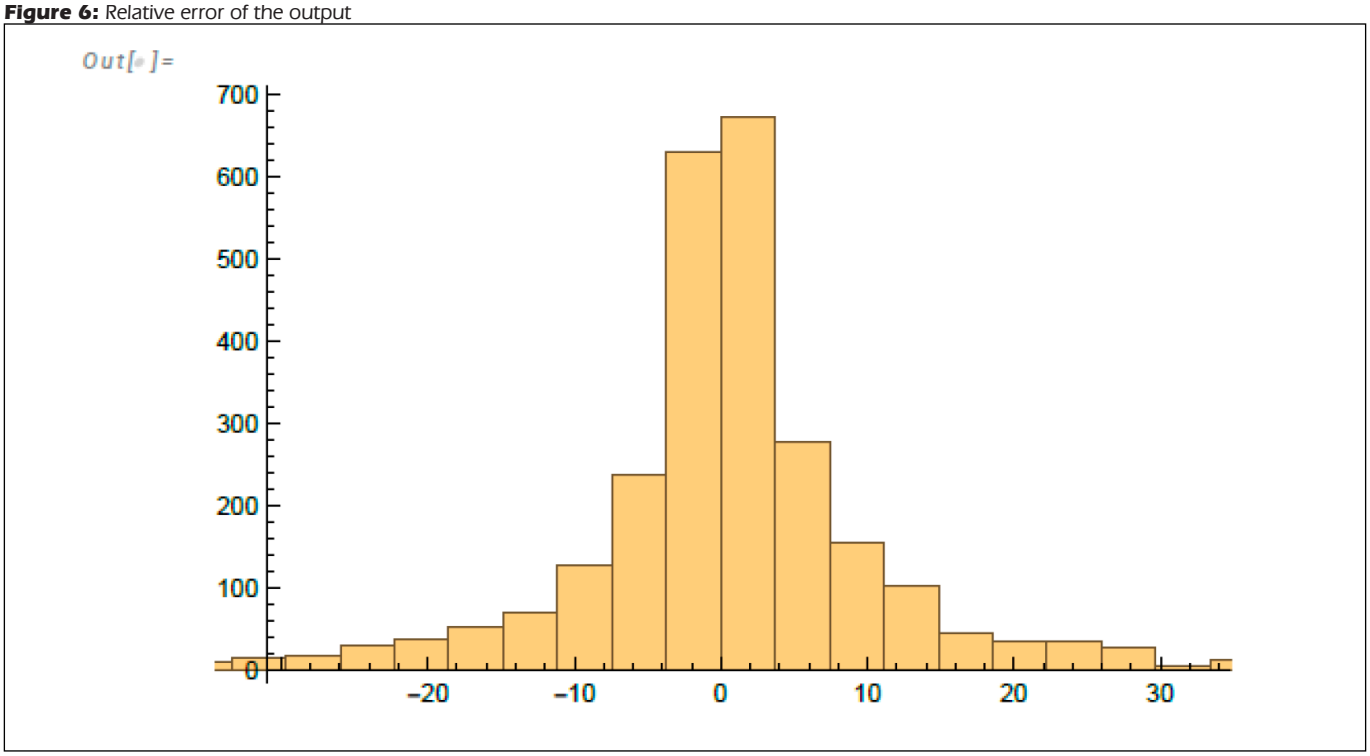

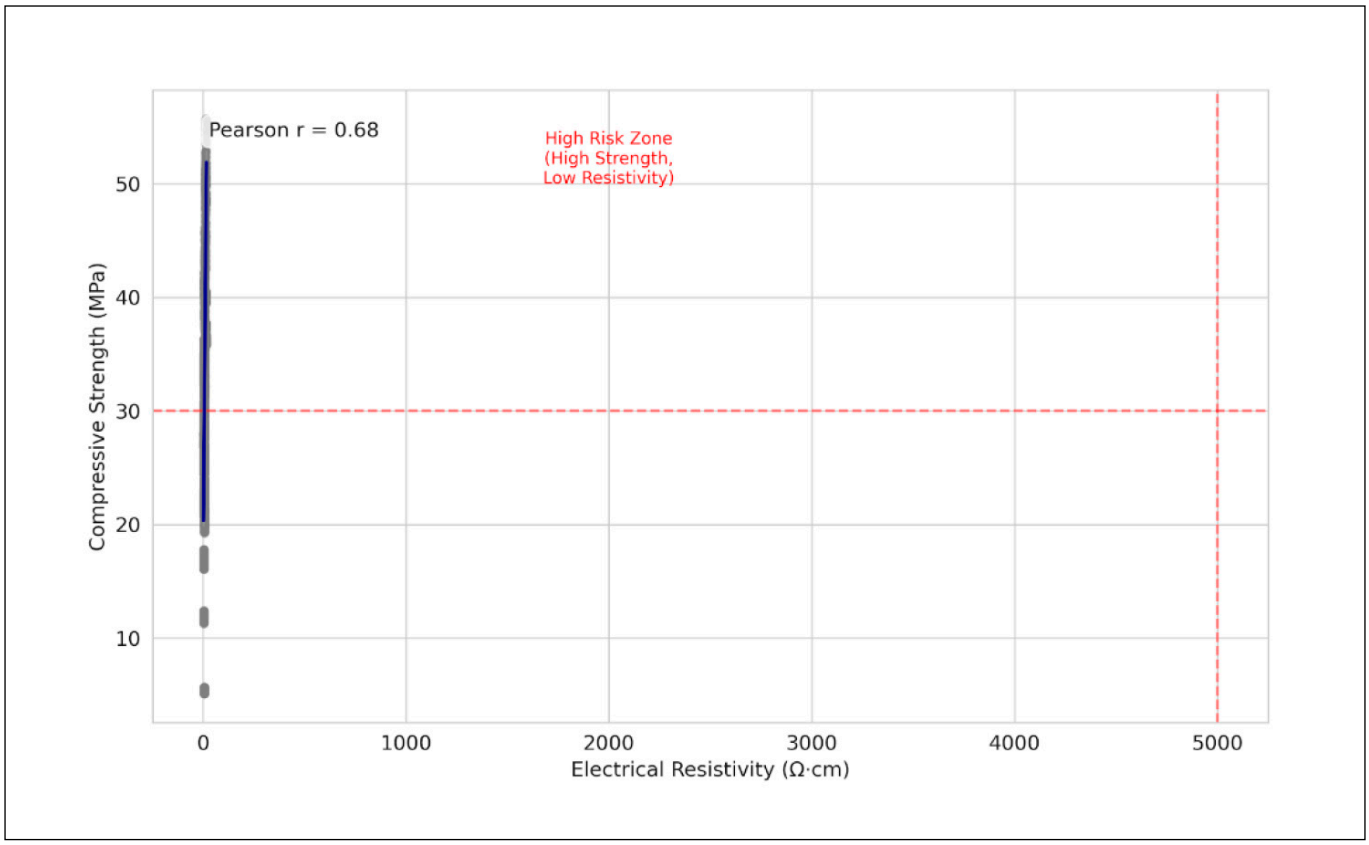

Figure 7: Correlation between measured Electrical Resistivity (E_r) and Compressive Strength (f'_c).

infrastructure (e.g., concrete made with Danube river aggregates) would require a transfer-learning step to recalibrate the baseline UPV and Resistivity values for local mineralogies.

- Surface vs. Core Decoupling in Aggressive Environments: The proposed NDT methods (UPV and Surface Resistivity) primarily assess the outer concrete layer. In aggressive acidic environments (pH < 4), the concrete surface may undergo softening or gypsum formation while the core remains intact. This "skin effect" could lead to a divergence between the NDT-predicted strength and the actual load-bearing capacity of the structural core over long exposure periods.

5. CONCLUSIONS AND FUTURE OUTLOOK

This study presented a comparative analysis of machine learning (ML) and deep learning (DL) methodologies for predicting the compressive strength of concrete. By processing a dataset of 4,420 NDT monitoring points through a computational framework in Wolfram Mathematica, we established that Artificial Intelligence offers a viable alternative to traditional single-variable regressions for quality control.

- Unified Durability-Strength Monitoring: The most significant finding is the validation of Electrical Resistivity as a dual-purpose indicator. In wastewater infrastructure, where durability against chemical attack is as critical as load-bearing capacity, this SNN model proves that resistivity readings can reliably predict compressive strength ($R^2 > 0.90$). This allows engineers to monitor both permeability (durability) and strength (structure) using a single non-destructive sensor.
- Resilience to Aggressive Aggregates: The model successfully generalized across concrete mixtures containing recycled and volcanic aggregates. This is vital for modern sustainable sewage systems, which increasingly utilize alternative binders and aggregates that often disrupt standard NDT calibration curves.
- Early Warning for Crack Formation: Since the model correlates Ultrasonic Pulse Velocity (UPV) with strength evolution, it effectively establishes a baseline for healthy concrete. Deviations from this AI-predicted baseline in the field can serve as an early warning system for micro-cracking or chemical degradation typical in industrial effluent environments.
- Future Outlook: Future work will integrate this algorithm into a Digital Twin framework for real-time monitoring of sewage pipes, specifically to quantify the impact of industrial effluent acidity on the long-term drift of NDT sensor readings.

6. NOTATIONS

- A_{type}: Aggregate type (categorical input)
- C_{type}: Cement type (categorical input)
- E_r: Electrical Resistivity (Ω/cm)
- f'_c: Compressive Strength (MPa)
- R^2 : Coefficient of Determination
- RMSE: Root Mean Squared Error
- SELU: Scaled Exponential Linear Unit (activation function)
- SNN: Self-Normalizing Neural Network
- Curing Age (days)
- Ultrasonic Pulse Velocity (m/s)

7. REFERENCES

ACI Committee 308 (2008). “Guide to Curing Concrete” (ACI 308R-01, Reapproved 2008). American Concrete Institute, Farmington Hills, MI.

Allahverdi, A., & Škvára, F. (2000). “Acidic corrosion of hydrated cement-based materials”. Ceramics – Silikáty, 44(3), 114–120.

Ghunimat, D., Alzoubi, A. E., Alzboon, A., & Hanandeh, S. (2023). “Prediction of concrete compressive strength with GGBFS and fly ash using multilayer perceptron algorithm, random forest regression and k-nearest neighbor regression”. Asian Journal of Civil Engineering, 24(1), 169–177.

Guzmán-Torres, J. A., Domínguez-Mota, F. J., Alonso-Guzmán, E. M., Tinoco-Guerrero, G., & Martínez-Molina, W. (2024). “ConcreteXAI: A multivariate dataset for concrete strength prediction via deep-learning-based methods”. Data in Brief, 53, 110218. https://doi.org/10.1016/j.dib.2024.110218 (Repository: https://github.com/JaGuzmanT/ConcreteXAI)

Klambauer, G., Unterthiner, T., Mayr, A., & Hochreiter, S. (2017). “Self-Normalizing Neural Networks”. Advances in Neural Information Processing Systems, 30, 971–980.

Massazza, F. (2002). “Pozzolana and pozzolanic cements”. In Lea’s Chemistry of Cement and Concrete (4th ed., pp. 471–631). Butterworth-Heinemann.

Mehta, P. K., & Monteiro, P. J. M. (2014). Concrete: Microstructure, Properties, and Materials (4th ed.). McGraw-Hill Education.

Mindess, S., Young, J. F., & Darwin, D. (2003). Concrete (2nd ed.). Prentice-Hall.

Moayedi, H., Eghtesad, A., Khajehzadeh, M., Keawsawasvong, S., Al-Amidi, M. M., & Le Van, B. (2022). “Optimized ANNs for predicting compressive strength of high-performance concrete”. Steel and Composite Structures, 44(6), 867–882.

MSZ 4798:2016 (2016). “Concrete. Specification, performance, production and conformity” (National Application Document of EN 206). Hungarian Standards Institution.

MSZ EN 1992-1-1:2010 (2010). “Eurocode 2: Design of concrete structures – Part 1-1: General rules and rules for buildings”. European Committee for Standardization.

Neville, A. M. (2011). Properties of Concrete (5th ed.). Pearson Education.

Scrivener, K. L., John, V. M., & Gartner, E. M. (2018). “Eco-efficient cements: Potential economically viable solutions for a low-CO2 cement-based materials industry”. Cement and Concrete Research, 114, 2–26.

Sobhani, J., Khanzadi, M., & Movahedian, A. H. (2013). “Support vector machine for prediction of the compressive strength of no-slump concrete”. Computers and Concrete, 11(4), 337–350.

Turk, K., & Karatas, M. (2011). “Abrasion resistance and mechanical properties of self-compacting concrete with different dosages of fly ash/silica fume”. Indian Journal of Engineering and Materials Sciences, 18(1), 49-60.

Valcuende, M., & Parra, C. (2010). “Natural products as a substitute for microsilica in high-performance concrete: Frost resistance”. Construction and Building Materials, 24(12), 2657-2663.

Zhang, K., Zhou, J., & Yin, Z. (2021). “Experimental study on mechanical properties and pore structure deterioration of concrete under freeze–thaw cycles”. Materials, 14(21), 6568.

Affes Hatem, (1996) MSc Structural engineer
Budapest University of Technology and Economics, Budapest, Hungary. From Sfax, Tunisia, currently pursuing his PhD at the Budapest University of Technology and Economics, Hungary. Having completed his Bachelor’s and Master’s degrees in Hungary over the past decade, his work focuses on sustainable construction. Contact: affeshatem@edu.bme.hu

Salem Georges Nehme, PhD. (1963)
Budapest University of Technology and Economics, Budapest, Hungary
Serves at the Budapest University of Technology and Economics, Hungary. Acting as a PhD supervisor, his research expertise centers on advanced construction materials and concrete durability. Contact: salem.nehme@emk.bme.hu

Béla Paláncz, D.Sc. (1944-2026)
Late Professor Emeritus Béla Paláncz was a distinguished researcher at the Budapest University of Technology and Economics. His extensive work specialized in mathematical computing, geospatial algebraic computations, and control engineering. His pioneering academic legacy continues to inspire the engineering community. Contact: N/A (Deceased)

Workshop Aims and History

AIMS: Collaboration of prestigiuos associations **ACI, *fib* and RILEM** aimed to harmonize design rules and **jointly develop future code specifications** in the emerging fields of FRC and UHPFRC.

HISTORY: RILEM has been already active at the beginning of 1990'-ies in FRC. Since 2010, the *fib* and ACI have been collaborating to strengthen ties between their technical communities. Their first focus area was Fibre Reinforced Concrete (FRC), where both organizations had active committee: **ACI Commissions 544, 239, 549** and ***fib* Task Group T4.1.** These collaborations has led to a series of successful international workshops in the field of *Fibre Reinforced Concrete – From Design to Structural Applications:*

- **FRC 2014, Montreal, Canada,** *Fibre Reinforced Concrete – From Design to Structural Applications*, Polytechnique Montreal. Proceedings published in **ACI SP-310** and ***fib* Bulletin 79** (Editors: Bruno Massicotte, J-Philippe. Charron, G. Plizzari, Barzin Mobasher).
- **FRC 2018, Desenzano, Italy, Fibre** *Reinforced Concrete – From Design to Structural Applications* – Proceedings published in **ACI SP-343** and ***fib* Bulletin 95** (Editors: Bruno Massicotte, Fausto Minelli, Barzin Mobasher, Giovanni Plizzari).
- **FRC 2023, Tempe, Arizona, USA, Fibre** *Reinforced Concrete – From Design to Structural Applications* – Publications forthcoming (Editors: B. Massicotte, B. Mobasher, G. Plizzari).

The foundation for these workshops date back to **2004** with the first International Workshop on Advances in Fibre Reinforced Concrete held in **Bergamo, Italy**, organized by Giovanni Plizzari and Marco di Prisco during BEFIB 2004. This event, supported by ACI, focused on developing structural design methodologies for FRC (Editors: S. Ahmad, Marco di Prisco, Christian Meyer, Giovanni Plizzari, Surendra Shah).

- **Catania, Italy, 2007** – FRAMCOS 6 Workshop, chaired by Carpinteri, Ferro, and Giovanni Plizzari. Published in *Materials & Structures* (2009, Special Issue).
- **Budapest, Hungary, 1999** – Early conference on FRC, organized by György L. Balázs, bringing together international researchers *on Fibre Reinforced Concrete – from research to practice* http://fib.bme.hu/konyvek/szalerositesu_betonok.pdf

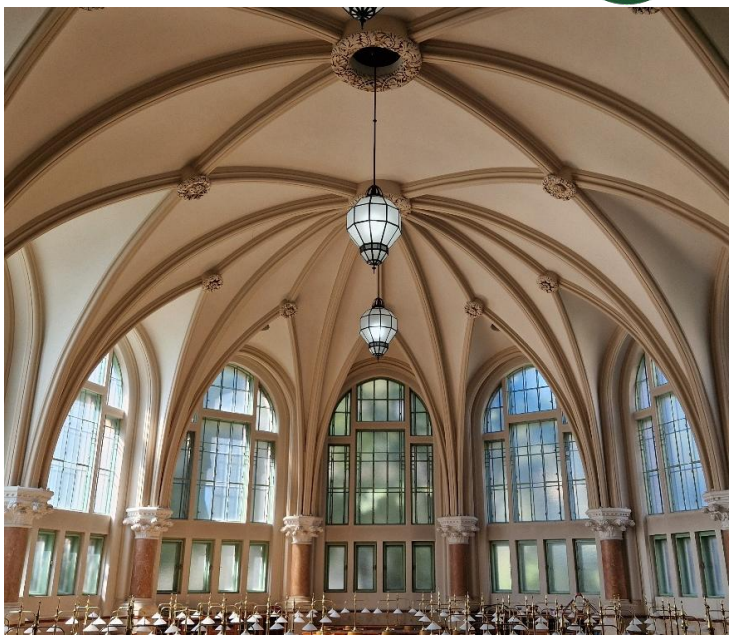

Library of the Budapest University of Tecnology and Ecconomics

Venue – BME Budapest

Budapest University of Technology and Economics was founded in 1782 and it has been regarded as Hungary's number one technical higher education institution for more than 240 years.

Budapest, resting gracefully along the Danube, harmonizes centuries of history with a vibrant present. Landmarks like Buda Castle and Matthias Church echo tales of the past, while District VII's lively atmosphere embodies modern creativity in its eclectic bars and cafes. Art and culture thrive here, from the grandeur of the Hungarian State Opera House to the avant-garde exhibitions at the Ludwig Museum.

Topics

1. Design specifications for applications
   - A. *fib* Model Code 2020
   - B. Standards and design specifications
   - C. Enhanced material behaviour and modelling
   - D. Enhanced structural behaviour and modelling in reinforced and in prestressed concrete members
2. Structural applications
   - A. Buildings, Bridges, Foundations
   - B. Tunnels
   - C. Prefabrication
   - D. Concrete industrial floors
3. Sustainability, Durability, Serviceability
   - A. Design aspects for sustainability and durability. Life Cycle Assessment.
   - B. Serviceability aspects: cracking, ~~first crack,~~ crack pattern, spacing of cracks, crack widths, increase of crack width
4. Design aspects for long term and extreme loads
   - A. Long term behaviour and modelling for shrinkage, creep, fatigue
   - B. FRC under fire, impact or blast loading.
5. Retrofitting and strengthening of existing structures
6. Fibres in new types of concretes and in 3D printed concretes

Sponsorship opportunities

We offer levels of sponsorship: Diamond (8,000 EUR), Gold (5,000 EUR), Silver (2,500 EUR), and Standard (1,000 EUR). Diamond and Gold sponsors receive exhibition space (larger for diamond). Diamond, Gold and Silver receive complimentary workshop registrations (4 for Diamond, 3 for Gold and 2 for Silver). All sponsors will have their logo displayed and name acknowledged during the opening and closing ceremonies, in the workshop proceedings, and on-site materials such as flyers and roll-ups. To become a sponsor, please provide your company details, and the sponsorship fee must be transferred prior to the workshop.

Additionally a Platinum sponsorship level is also considerded and prize is assigned on special topic proposed by the Sponsor.

Joint publication

The Workshop will conclude by a joint publication being part of the fib Series Proceedings (that is going to index by Scopus) as well as a Special Publication by ACI. We are also looking for a Summary of results for RILEM.

Contact information

Official website:

https://frcworkshop2026.bme.hu

Műegyetem 3, Budapest, H-1111 Hungary

frcworkshop2026@emk.bme.hu

AZ NKFI ALAPBÓL MEGVALÓSULÓ PROJEKT
NEMZETI KUTATÁSI, FEJLESZTÉSI ÉS INNOVÁCIÓS HIVATAL
AZ INNOVÁCIÓ LENDÜLETE

BME, *consortium leader*
SW Umwelttechnik Mo. Kft.,
ÉMI Nonprofit Kft. MC Bauchemie.
CRH Mo. Kft.

MŰEGYETEM 1782
BUDAPESTI MŰSZAKI ÉS GAZDASÁGTUDOMÁNYI EGYETEM
Építőmérnöki Kar - építőmérnöki képzés 1782 óta
Építőanyagok és Magasépítés Tanszék

National Competitiveness and Excellence Program, Subprogram B:National Program for Materials Science and Technology
Hungarian Research Grant NVKP_16-1-2016-0019
"Development of concrete products with improved resistance to chemical corrosion, fire or freeze-thaw"."
Procurement of laboratory equipment within the framework of the tender entitled

Project supervisor: Prof. György L. Balázs

Project sub-theme responsibles: Dr. Éva Lublóy, Dr. Salem G. Nehme, Dr. Katalin Kopecskó

MATERIAL SCIENTIFIC STUDIES FROM NANO-LEVEL TO MACRO-LEVEL

1. PHENOM XL Scanning Electron Microscope (SEM) with elemental analysis of EDS (energy dispersive X-ray spectroscopy) for small and large (max. 100 mm x 100 mm) samples

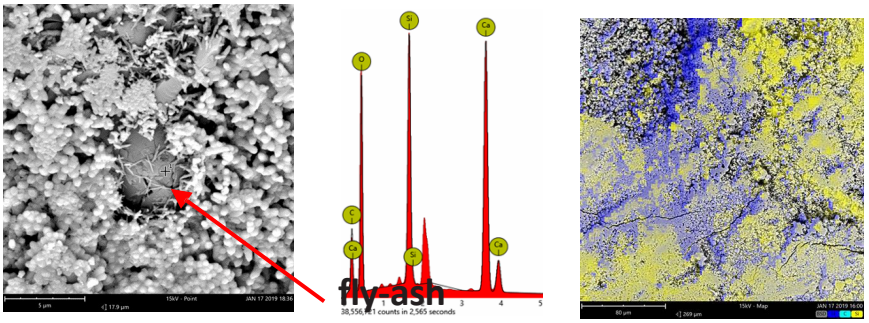

2. TAM Air 3+3 channel microcalorimeter, with 125 ml ampoulles, application range: from cement paste to concrete

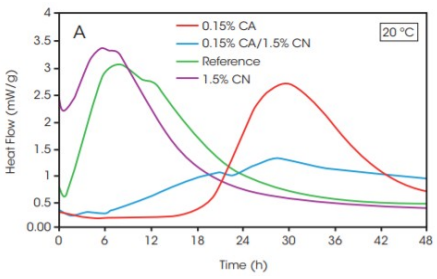

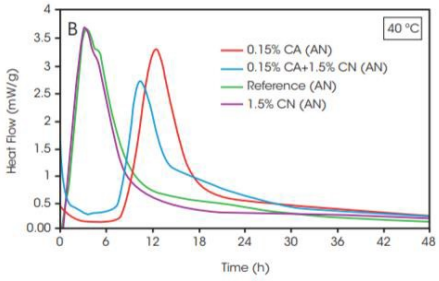

3. Zetasizer Nano ZS – Measurement of Zeta potential with titrator (variable pH range) 3,8 nm – 100 µm, particle size distribution in range 0,3 nm – 10 µm